

## An earliest Paleocene squirrelfish (Teleostei: Beryciformes: Holocentroidea) and its bearing on the timescale of holocentroid evolution

James V. Andrews, Jason P. Schein & Matt Friedman

To cite this article: James V. Andrews, Jason P. Schein & Matt Friedman (2023) An earliest Paleocene squirrelfish (Teleostei: Beryciformes: Holocentroidea) and its bearing on the timescale of holocentroid evolution, *Journal of Systematic Palaeontology*, 21:1, 2168571, DOI: [10.1080/14772019.2023.2168571](https://doi.org/10.1080/14772019.2023.2168571)

To link to this article: <https://doi.org/10.1080/14772019.2023.2168571>



© 2023 The Author(s). Published by Informa UK Limited, trading as Taylor & Francis Group.



[View supplementary material](#)



Published online: 03 Mar 2023.



[Submit your article to this journal](#)





[View related articles](#)



[View Crossmark data](#)



# An earliest Paleocene squirrelfish (Teleostei: Beryciformes: Holocentroidea) and its bearing on the timescale of holocentroid evolution

James V. Andrews<sup>a,b,\*</sup> , Jason P. Schein<sup>c</sup> and Matt Friedman<sup>a,b</sup> 

<sup>a</sup>Department of Earth & Environmental Sciences, University of Michigan, 1105 North University Ave, Ann Arbor, Michigan 48109-1382, USA; <sup>b</sup>Museum of Paleontology, University of Michigan, 3102 Biological Sciences Building, Ann Arbor, Michigan 48109-1382, USA; <sup>c</sup>Elevation Science Institute for Natural History Exploration, PO Box 672, Red Lodge, Montana 59068, USA

(Received 26 July 2022; accepted 9 January 2023)

The record of articulated marine fish fossils during the latest Cretaceous and earliest Cenozoic is sparse. The oldest-known definitive squirrelfishes and soldierfishes, like the first examples of many extant reef-dwelling clades, are known from early Eocene deposits of Europe. Here, we describe a new genus and species of holocentroid (Teleostei: Beryciformes: Holocentroidea) based on material from three individuals from early Paleocene (Danian) deposits of New Jersey, USA using micro-computed tomography. The specimens comprise a three-dimensionally preserved skull and partial postcranium, plus two isolated neurocrania. The new taxon, †*Iridopristsis parrisi*, possesses a unique combination of characters, including a heterosulcoid otolith morphology and an edentulous premaxillary tooth-gap, while lacking a newly proposed character for the remainder of Cenozoic holocentroids: a lamina on the lateral surface of the anguloarticular, anterior to the jaw joint. Bayesian phylogenetic analysis of morphological, stratigraphical and molecular data under the fossilized birth-death process finds that the new taxon branches from the holocentroid stem, where it is joined by two of the three squirrelfish genera from the early Eocene (Ypresian) of Bolca, Italy. We estimate a Danian divergence between Myripristinae and Holocentrinae, the two reciprocally monophyletic subfamilies of Holocentridae. Our analysis suggests that several holocentroid lineages crossed the Cretaceous–Palaeogene boundary.

<http://zoobank.org/urn:lsid:zoobank.org:pub:0B458336-EFCF-46D0-98D0-CE5AD371D7AF>

**Keywords:** Acanthomorpha; Cretaceous–Palaeogene boundary; squirrelfishes; computed tomography; Bayesian phylogenetics; parsimony

## Introduction

Holocentridae (squirrelfishes and soldierfishes) comprises nearly 90 extant species of primarily reef-dwelling, nocturnal spiny-rayed fishes (Nelson et al., 2016). Holocentrids are frequently resolved as, or within, the sister lineage to the species-rich and morphologically diverse percomorph fishes, a clade comprising approximately 25% of all vertebrate species (Alfaro et al., 2018; Betancur-R. et al., 2017; Davesne et al., 2016; Dornburg et al., 2017; Dornburg & Near, 2021; Hughes et al., 2018; Miya et al., 2003; Nelson et al., 2016; Stiassny & Moore, 1992). The group includes two lineages of roughly equal species richness: the generally shallower-water squirrelfishes (Holocentrinae) and the generally deeper-living soldierfishes (Myripristinae) (Nelson et al., 2016).

The body fossil record of Holocentroidea (herein referring to the total-group of Holocentridae and all fossil lineages more closely related to the extant family than other members of Beryciformes) consists of two

parts, separated by a stratigraphical gap. The first of these comprises the Eocene–Recent interval, which yields multiple genera closely associated with – or clearly belonging within – the holocentroid crown (Dornburg et al., 2015). The best-known body fossils of Cenozoic holocentroids come from the famous Eocene (Ypresian) Lagerstätte of Bolca, Italy, where the group is represented by three species: †*Eoholocentrum macrocephalum* (Blainville, 1818), †*Berybolcensis leptacanthus* (Agassiz, 1838) and †*Tenuicentrum lanceolatum* (Bassani, 1876) Sorbini, 1975 (Friedman & Carnevale, 2018; Sorbini, 1975a, b, 1979a, b; Sorbini & Tirapelle, 1975). They are joined by additional specimens from the Eocene of Italy, Florida in the USA and possibly the UK (Casier & Stinton, 1966; Dunkle & Olsen, 1959; Marramà et al., 2021), along with the Miocene of the Mediterranean Basin (Bassani, 1911). These fossils are potentially significant in constraining shifting geographical patterns of marine biodiversity in the Cenozoic (Dornburg et al., 2015).

\*Corresponding author. Email: [jamesva@umich.edu](mailto:jamesva@umich.edu)

The Eocene and younger set of holocentroid fossils are separated from an older series of taxa from Late Cretaceous deposits. These Cretaceous forms are not members of Holocentridae, and are instead interpreted as holocentroids. Examples include representatives from the Cenomanian of Lebanon (Gaudant, 1969; Patterson, 1967), Cenomanian–Turonian of the UK (Patterson, 1964), Turonian of Brazil (Gallo-da-Silva & De Figueiredo, 1999) and the Santonian of Mexico and the USA (Alvarado-Ortega & Than-Marchese, 2013; Bardack, 1976). A 35 Myr gap extending from the middle of the Late Cretaceous to the early Eocene separates these two parts of the holocentroid fossil record. This hiatus reflects the general rarity of articulated marine fishes around the Cretaceous–Palaeogene boundary (Argyriou & Davesne, 2021; Patterson, 1993; but see Carranza-Becerra, 2020, as well as Alvarado-Ortega *et al.*, 2015). As for other groups of acanthomorphs (Alfaro *et al.*, 2018; Friedman, 2010), this interval appears to be an important episode in the evolutionary history of holocentroids. Information on fossils from this time is likely to have important implications for the timing of the origin of Holocentridae and the innovations of its two major lineages, as well as patterns of phylogenetic survivorship over the end-Cretaceous mass extinction.

Here we use micro-computed tomography ( $\mu$ CT) to describe a new genus and species of holocentroid that falls within this conspicuous stratigraphical gap. Represented by a nearly complete skull plus incomplete postcranium and two referred neurocrania from the earliest Paleocene (Danian) of New Jersey, USA, it is the earliest holocentroid skeleton from the Cenozoic and a rare example of three-dimensionally preserved marine teleost remains from the Danian. We include the new taxon in a combined analysis of extant and fossil holocentroids with the goals of inferring its phylogenetic position and estimating the timescale of holocentroid evolution.

## Material and methods

### Specimen imaging

**Computed tomography.** Materials were imaged using the Nikon XT H 225 ST industrial CT scanners at the University of Michigan Department of Earth and Environmental Sciences CTEES facility and at the Natural History Museum, London. Reconstructed dataset segmentation and visualization was carried out using Mimics v. 19.0 (Materialise, Belgium). Figured bones were exported as surface (.ply) files and rendered in Blender v. 2.91 (blender.org). Raw tomograms (.tif),

surface files of segmented elements (.ply format) and the Materialise Mimics file (.mcs) are available on Figshare (10.6084/m9.figshare.21754541).

**Photogrammetry.** Photogrammetric models were generated at the University of Michigan Research Museums Center following University of Michigan Online Repository of Fossils (UMORF) methodology (<https://umorf.ummp.lsa.umich.edu/wp/about/project-methods/>).

### Institutional abbreviations

Institutional abbreviations follow those of Sabaj (2020). **AMNH FF**, American Museum of Natural History fossil fishes, New York, NY, USA; **ANSP**, The Academy of Natural Sciences of Philadelphia, Philadelphia, PA, USA; **FMNH**, Field Museum of Natural History, Chicago, IL, USA; **FMNH P/PF**, Field Museum of Natural History palaeontological collections, Chicago, IL, USA; **NHMUK P**, The Natural History Museum palaeontological collection, London, UK; **NJSM GP**, New Jersey State Museum palaeontological collection, Trenton, NJ, USA; **UMMZ**, University of Michigan Museum of Zoology, Ann Arbor, MI, USA; **YPM VP**, Yale University, Peabody Museum of Natural History palaeontological collection, New Haven, CT, USA.

### Dagger symbol

The obelus ( $\dagger$ ) indicates extinct taxa, following Patterson and Rosen (1977).

### Comparative material

**Berycidae.** *Beryx splendens* Lowe, 1834 UMMZ 142822; *Centroberyx affinis* (Günther, 1859) UMMZ 216732.

**Holocentroidea.** *Corniger spinosus* Spix *et al.*, 1829–1831 ANSP 144596; *Flammeo marianus* (Cuvier, 1829) FMNH 77737; *Holocentrus rufus* (Walbaum, 1792) UMMZ 172341; *Myripristis murdjan* (Forsskål, 1775) UMMZ 185696; *Plectrypops retrospinis* (Guichenot, 1853) UMMZ 176518; *Pristilepis oligolepis* (Whitley, 1941) FMNH 73568; *Sargocentron rubrum* (Forsskål, 1775) UMMZ 245614;  $\dagger$ *Berybolcensis leptacanthus* FMNH PF 3215;  $\dagger$ *Caproberyx superbus* (Dixon, 1850) NHMUK P 5686;  $\dagger$ *Eoholocentron macrocephalum* FMNH P 25310,  $\dagger$ *Myripristis homopterygius* Agassiz, 1839 FMNH PF 3212, 3434.

**Melamphaidae.** *Scopelogadus beanii* (Günther, 1887) UMMZ 22771, *Scopelogadus bispinosus* (Gilbert, 1915) UMMZ 176339.

**Monocentridae.** *Monocentris japonica* (Houttuyn, 1782) UF 159787.

**Trachichthyidae.** *Hoplostethus mediterraneus* Cuvier, 1829 UMMZ 20406, *Gephyroberyx japonicus* (Döderlein in Steindachner & Döderlein, 1883) UMMZ 180097.

In addition to direct examination of fossil material, we also evaluated some characters based on the following descriptions: Patterson (1964); Sorbini (1975a, b, 1979a, b); Stewart (1984).

### Phylogenetic analysis

**Dataset assembly.** The character matrix is adapted from that of Dornburg et al. (2015), itself a modification of Stewart's (1984) phylogenetic analysis of holocentroid fishes. Stewart's matrix incorporates characters from Nelson (1955), Dunkle & Olsen (1959), Patterson (1968), Woods & Sonoda (1973), Sorbini (1975a, b, 1979a, b), Zehren (1979), Gayet (1980a, b) and Randall et al. (1982). The Stewart (1984) matrix originally comprised 72 characters. Dornburg et al. (2015) added eight further characters, with codings derived principally from Moore (1993). Based on our study of the new fossil taxon, we developed two novel characters and added them to this matrix. These characters are described in more detail in the Results section. The final morphological matrix contains 82 characters across 18 fossil and living taxa.

A concatenated and aligned molecular dataset comprising 23 outgroup species from the families Polymixiidae, Trachichthyidae and Berycidae, and 43 species of the in-group family Holocentridae were retrieved from the R package 'fishree' (Rabosky et al., 2018; Chang et al., 2019). Of the species with morphological characters scored, only *Corniger spinosus* and *Pristilepis oligolepis* lacked molecular data in this alignment. The final molecular alignment comprised the following genes: 12s, 16s, 4c4, coi, cytb, enc1, ficd, glyt, hoxc6a, kiaa1239, myh6, panx2, plagl2, ptr, rag1, rhodopsin, ripk4, sh3px3, sidkey, sreb2, svep1, tbr1, vcpip and zic1. Indeterminate partitions for the sampled taxa were manually removed from the original 'fishree' alignment using Aliview (Larsson, 2014), and included the genes nd2 (alignment positions 8822–9868 in the 'fishree' alignment), nd4 (alignment positions 9869–11401), and rag2 (alignment positions 15117–16340). The molecular and morphological matrices were then manually concatenated in a text editor. Dornburg et al. (2012) established a new taxonomical framework for Holocentrinae to address non-monophyly of the genera *Neoniphon* and *Sargocentron*. As such, we use the binomial combinations established by Dornburg et al. (2012)

for members of Holocentrinae, rather than those within the 'fishree' package.

**Parsimony analysis.** We analysed the morphological character matrix under maximum parsimony in PAUP\* v. 4.0a169 (Swofford, 2003). A heuristic search was performed (addseq=random, hold = 5, nreps = 500, swapping algorithm=TBR) with unweighted and unordered characters, and multistate characters set as variable. Bootstrapping was performed in PAUP\* (nreps = 100) to obtain nodal support values, retaining clades with greater than 50% frequency. The analysis was rooted on *Polymixia berndti* Gilbert, 1905 based on prior hypotheses of acanthomorph interrelationships (Johnson & Patterson, 1993; Dornburg & Near, 2021). Bremer support values were manually calculated in PAUP\* by computing a strict consensus tree, then sequentially increasing the maximum number of steps per tree kept until all branches collapsed into a polytomy. An agreement subtree was generated in PAUP\* for the most parsimonious trees to determine which taxa were acting as phylogenetic rogues within the analysis.

**Character state optimization.** The agreement subtree generated in PAUP\* and a modified morphological character matrix comprising only those taxa within the agreement subtree were imported into MacClade (Maddison & Maddison, 2000) to visualize character state optimizations.

**Bayesian analysis.** We used the combined morphological and molecular dataset to conduct a fossilized birth-death analysis in MrBayes v. 3.2.7 (Heath et al., 2014; Huelsenbeck & Ronquist, 2001; Zhang et al., 2016). Molecular data were split into 34 partitions and a best fit substitution model was estimated for each partition in the alignment using PartitionFinder2 (Guindon et al., 2010; Lanfear et al., 2012, 2017) on the CIPRES Science Gateway web server (Miller et al., 2010). Morphological data used the default MrBayes modification of the Mkv model (Lewis, 2001) with gamma-distributed substitution rates. As in parsimony analyses, *Polymixia berndti* was assigned as the outgroup. †*Caproberyx* was constrained to the in-group comprising trachichthyids, berycids and holocentrids based on a longstanding hypothesis of holocentroid affinity (Johnson & Patterson, 1993; Murray, 2016; Patterson, 1964; Regan, 1911). The tree age prior was assigned an offset exponential distribution between 100.5 and 153 Ma. The upper bound is based on the highest posterior density (HPD) intervals of recent node-calibrated molecular estimates for the age of the acanthomorph crown (Alfaro et al., 2018; Hughes et al., 2018), while the lower bound is based on the earliest occurring acanthomorphs, deriving from Muhi Quarry of the late

Albian-age El Doctor Formation in Hidalgo, Mexico (López-Palomino *et al.*, 2021). Fossil age calibrations are justified in [Supplemental Material – File 1](#). It is clear that well-preserved fossil fishes are not uniformly distributed with respect to stratigraphy, with many authors noting strong Lagerstätten effects in the teleost record (e.g. Patterson, 1993). In the context of our analysis, the Ypresian deposits of Bolca represent an exceptional window of preservation, with three different holocentroid genera recovered from the same deposit. To reflect this uneven sampling, we designated intervals with differing fossilization probabilities before, during and after the Ypresian. The analysis included two independent runs on four chains of 30 million generations each, with samples being taken every 100 generations. The first quarter of samples were discarded as burn-in. Convergence was determined by split frequencies reaching below 0.01, and by visually inspecting the marginal probability distribution and trace of the analysis in Tracer v. 1.7.2 (Rambaut *et al.*, 2018).

## Geological context

The Hornerstown Formation comprises glauconitic greensands and includes the Cretaceous–Palaeogene boundary. The formation extends approximately 150 kilometres from the Atlantic Coast in north-east New Jersey to the Delaware River in south-west New Jersey (Fig. 1A). Greensand deposits re-emerge in Delaware and Maryland, where they are occasionally exposed along downcutting stream banks (Higgins & Conant, 1986; Tomlinson & Ramsey, 2020). The Hornerstown Formation ranges in thickness between 1.5 and 7 metres, and in Sewell, New Jersey overlies the Navesink Formation of Maastrichtian age, and underlies the Vincentown Formation of Thanetian age (Owens *et al.*, 1999) (Fig. 1B). The Hornerstown Formation includes a 10-cm-thick bed known as the ‘Main Fossiliferous Layer’ (MFL) located 20 cm above the contact with the Navesink Formation (Gallagher, 2002; Koch & Olsson, 1977; Parris, 1974; Voegelé *et al.*, 2021). The specimens described here were collected by David Parris in 1979 from the MFL exposed in the Inversand Quarry in Sewell, New Jersey, USA. This locality has since been acquired by Rowan University and designated as the Jean and Ric Edelman Fossil Park.

Gallagher (2002) lists the macrofauna within the MFL of the Hornerstown Formation, including brachiopods, bivalves, gastropods, nautiloids, ammonoids, crustaceans, chondrichthyans, ray-finned fishes, turtles (including articulated individuals; Boles, 2016; Ullmann & Carr, 2021), crocodylians, mosasaurs and birds.

Actinopterygians include the acipenseriform *Acipenser*, the aulopiform †*Enchodus*, and the tselfatiiform †*Bananogmius*, along with indeterminate teleost vertebrates. Additionally, plant material (including casts of wood-boring bivalves) is found in relatively high abundance approximately 32 cm above the Hornerstown–Navesink contact (Voegelé *et al.*, 2021).

Attempts at radiometric dating of the Navesink, Hornerstown and Vincentown formations using potassium-argon and rubidium-strontium systems have provided inadequate age estimates. This is due to glauconitic units being open systems unfit for radiometric dating, resulting in systematically younger ages than anticipated in the light of geological and biostratigraphical data (Gallagher, 2002; Gallagher & Parris, 1996; Owens & Sohl, 1973). Historically, the age of the MFL of the Hornerstown Formation has been contentious due to varying biostratigraphical (Gallagher, 2002; Gallagher *et al.*, 2012; Koch & Olsson, 1977) and geological evidence, with working definitions of the MFL itself causing confusion (Voegelé *et al.*, 2021).

Recent evidence suggests that the MFL may comprise a death assemblage dating to or near the K/Pg extinction event (Ullmann *et al.*, 2018). Evidence includes shocked quartz found in burrows at the intersection of the MFL and the underlying Navesink Formation (Obasi *et al.*, 2011), and a diffuse iridium layer present midway through the height of the MFL bed. This suggests the Cretaceous fauna found within the MFL (e.g. mosasaurs) is reworked into an *in situ* Palaeogene fauna (Esmeray-Senlet *et al.*, 2017). Here, we assume an earliest Danian age for the holocentroid specimens described here, accepting the interpretations of Gallagher (1995) and Kennedy & Cobban (1996) that taphonomically worn Cretaceous-age taxa have been reworked into an earliest Cenozoic matrix. The articulation of the holotype specimen is inconsistent with such reworking, and thus suggests a Danian age (D. Parris, pers. comm., 2020).

There are previous reports of other, less informative remains of possible holocentroids from the latest Cretaceous and earliest Palaeogene deposits of New Jersey. These include a three-dimensionally preserved body fossil lacking the skull and caudal regions from the Maastrichtian ‘lower green sand-bed’ of the Navesink Formation in Monmouth County, New Jersey, described by Edward D. Cope (1869) (Rapp, 1946), and isolated dorsal fin spines, pterygiophores, and opercular elements collected at the boundary of the Maastrichtian New Egypt Formation and the Hornerstown Formation at Crosswicks Creek in Upper Freehold County, New Jersey (Becker *et al.*, 2009). Cope’s (1869) body fossil (AMNH FF 7530) is the type of †*Beryx* ‘*insculptus*’ Cope, 1869, but has no obvious diagnostic characters.

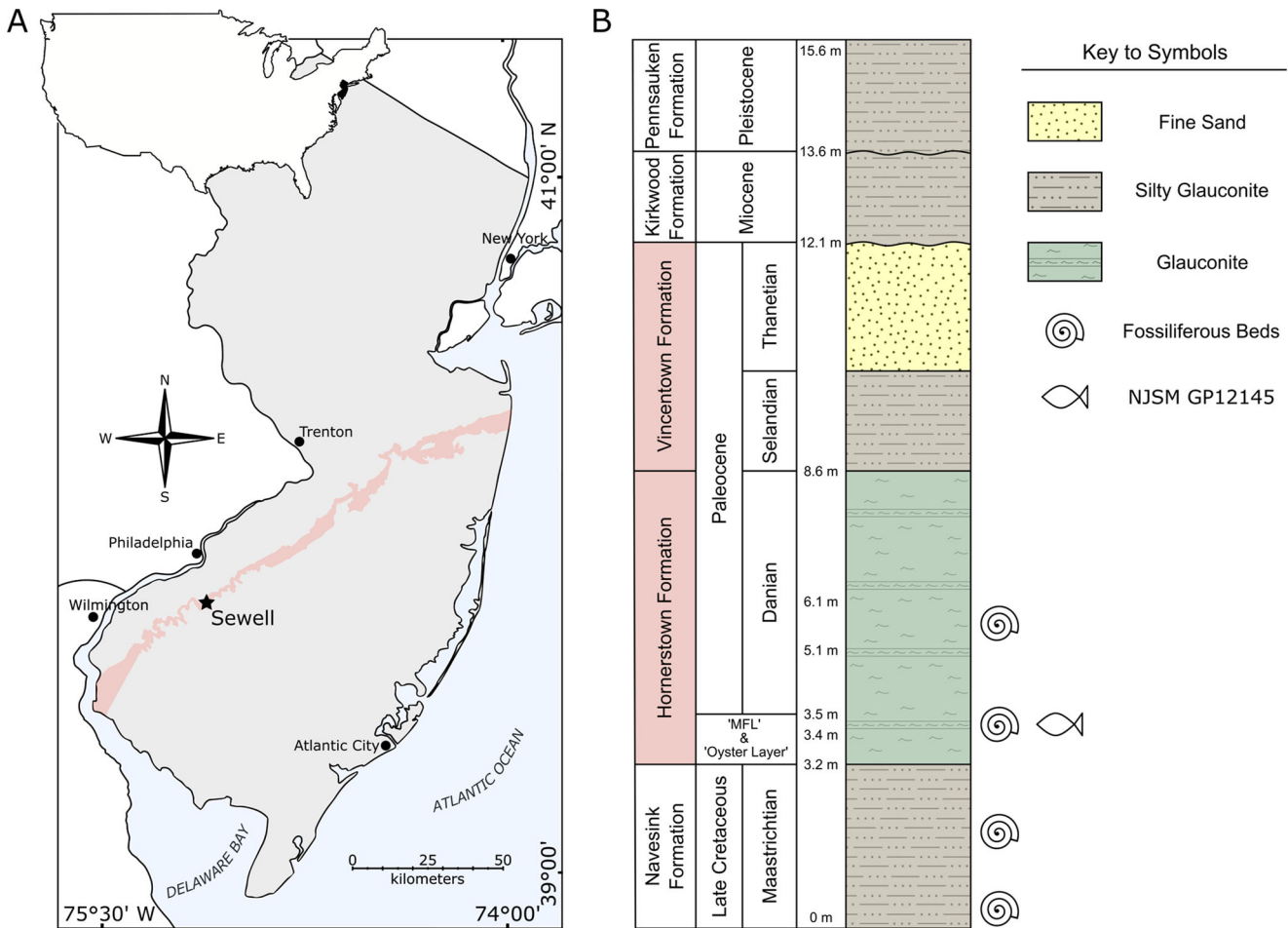


**Figure 1.** The geological setting of NJSM GP12145. **A**, outline of the USA with the state of New Jersey highlighted in black overlaying map with New Jersey highlighted in grey. Coral highlighting the combined Hornerstown and Vincentown formations. Fossil locality, the Jean and Ric Edelman Fossil Park, in Sewell marked with a black star. Adapted from Owens et al. (1999) and Dalton et al. (2014). **B**, stratigraphical section at the Jean and Ric Edelman Fossil Park. NJSM GP12145 derives from the Danian portion of the Main Fossiliferous Layer of the Hornerstown Formation. The combined Hornerstown and Vincentown formations are highlighted in coral. Adapted from Staron et al. (2001).

The isolated dorsal fin elements of Becker et al. (2009) remain unnamed. Cope (1869) discusses a second specimen of his †*Beryx insculptus* recovered from the ‘dark clay marl’ of Hornerstown, New Jersey and subsequently sent to Othniel C. Marsh at Yale.

It is unclear whether this second specimen was the partially articulated skull and postcranium (YPM VP 007260) from the Campanian Marshalltown Formation in Swedesboro, Gloucester County, New Jersey that was deposited by Othniel Marsh in 1869 at the Peabody Museum of Natural History at Yale University. Unfortunately, this specimen was inadvertently destroyed and was never formally described. Photos of the American Museum and Yale Peabody specimens are available in Supplemental Material Figure 1.

## Systematic palaeontology

Infraclass **Teleostei** Müller, 1845  
 Subsection **Acanthomorphata** Rosen, 1973  
 Order **Beryciformes** Regan, 1911 *sensu* Dornburg & Near, 2021  
 Superfamily **Holocentroidea** Richardson, 1846 *sensu* Gayet, 1980b  
 Genus †*Iridopristsis* gen. nov.

**Diagnosis.** As for type and only species.

†*Iridopristsis parrisi* sp. nov.  
 (Figs 2–15)



**Figure 2.** Photogrammetric model of the skull of †*Iridopristsis parrisi*, gen. et sp. nov., holotype (NJSM GP12145), Hornerstown Formation, early Paleocene (Danian), New Jersey, USA.

**Diagnosis.** Holocentroid with the unique combination of the following characters: orbital branch of the supra-orbital sensory canal with a separate opening from the main channel of the canal; large supraoccipital crest which is triangular in lateral aspect and borders the foramen magnum; parasphenoid with ventrolateral wings; lack of a berycimorph foramen in the anterior ceratohyal; deeply notched ventral surface of the anterior

ceratohyal to accommodate branchiostegals; elongate postmaxillary process of the premaxilla; maxillary shaft approximately cylindrical in cross-section and elongate; presence of an alveolar platform expanded outwardly at the symphyseal area of the dentary; distinct edentulous concavity along the mesial margin of the premaxilla; unornamented triangular facet present on the posterolateral surface of the maxilla; edentulous ectopterygoid;

A



B

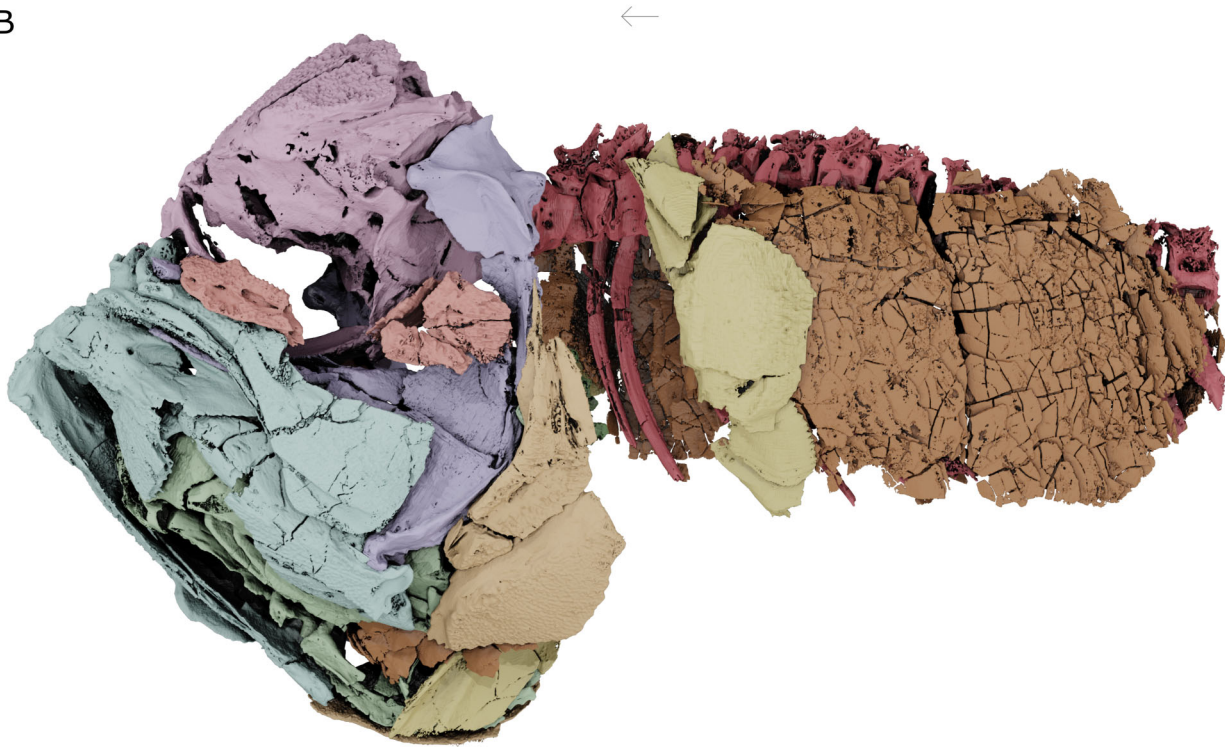


**Figure 3.** Skull and abdomen of †*Iridopristis parrisi* in left lateral view. Holotype (NJSM GP12145), Hornerstown Formation, early Paleocene (Danian), New Jersey, USA. **A**, specimen photograph and **B**, rendered  $\mu$ CT model. Skeletal regions highlighted as follows: neurocranium (pink), suspensorium (purple), circumorbitals (coral), jaws (light blue), opercles (light orange), ventral hyoid (light green), gill skeleton (dark green), pectoral girdle (yellow), abdominal scales (dark orange), vertebral column (red). Arrow indicates anatomical anterior. Scale bar represents 5 cm.



A



B

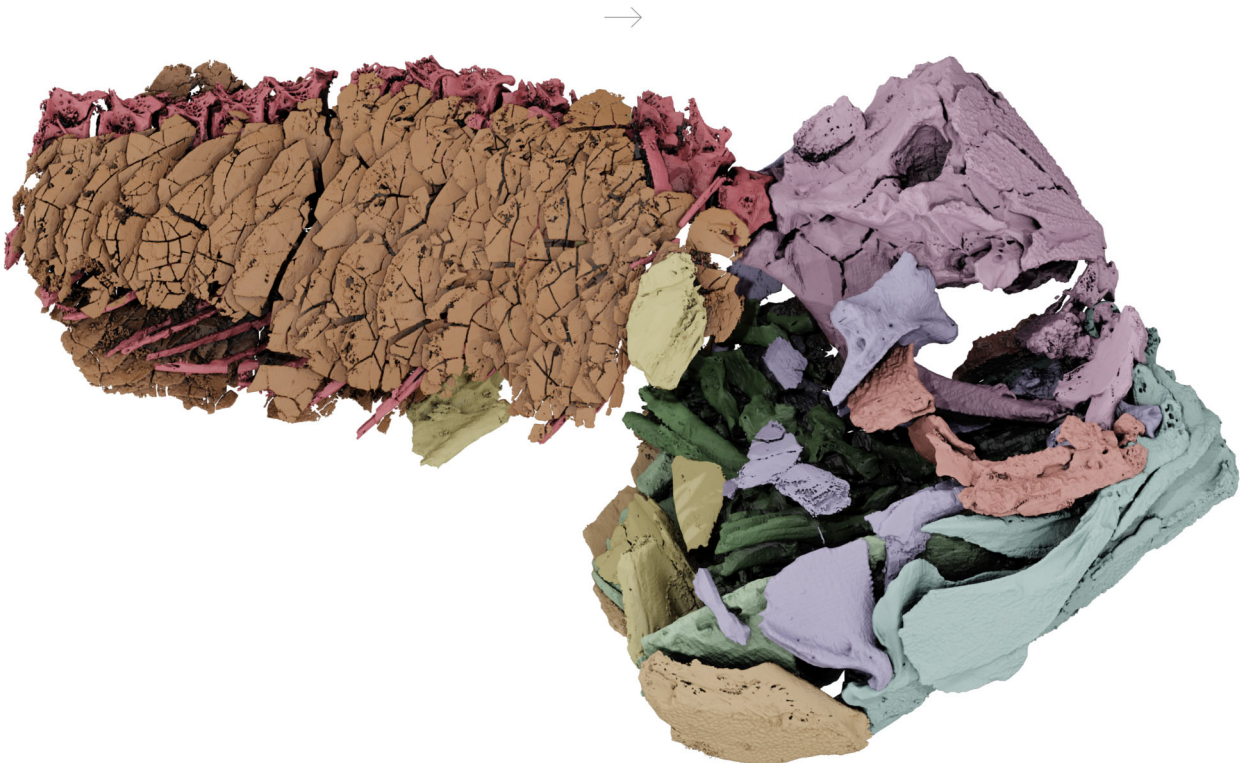


**Figure 4.** Skull and abdomen of †*Iridopristsis parrisi* in right lateral view. Holotype (NJSM GP12145), Hornerstown Formation, early Paleocene (Danian), New Jersey, USA. **A**, specimen photograph and **B**, rendered  $\mu$ CT model. Skeletal regions highlighted as follows: neurocranium (pink), suspensorium (purple), circumorbitals (coral), jaws (light blue), opercles (light orange), ventral hyoid (light green), gill skeleton (dark green), pectoral girdle (yellow), scales (dark orange), vertebral column (red). Arrow indicates anatomical anterior. Scale bar represents 5 cm.

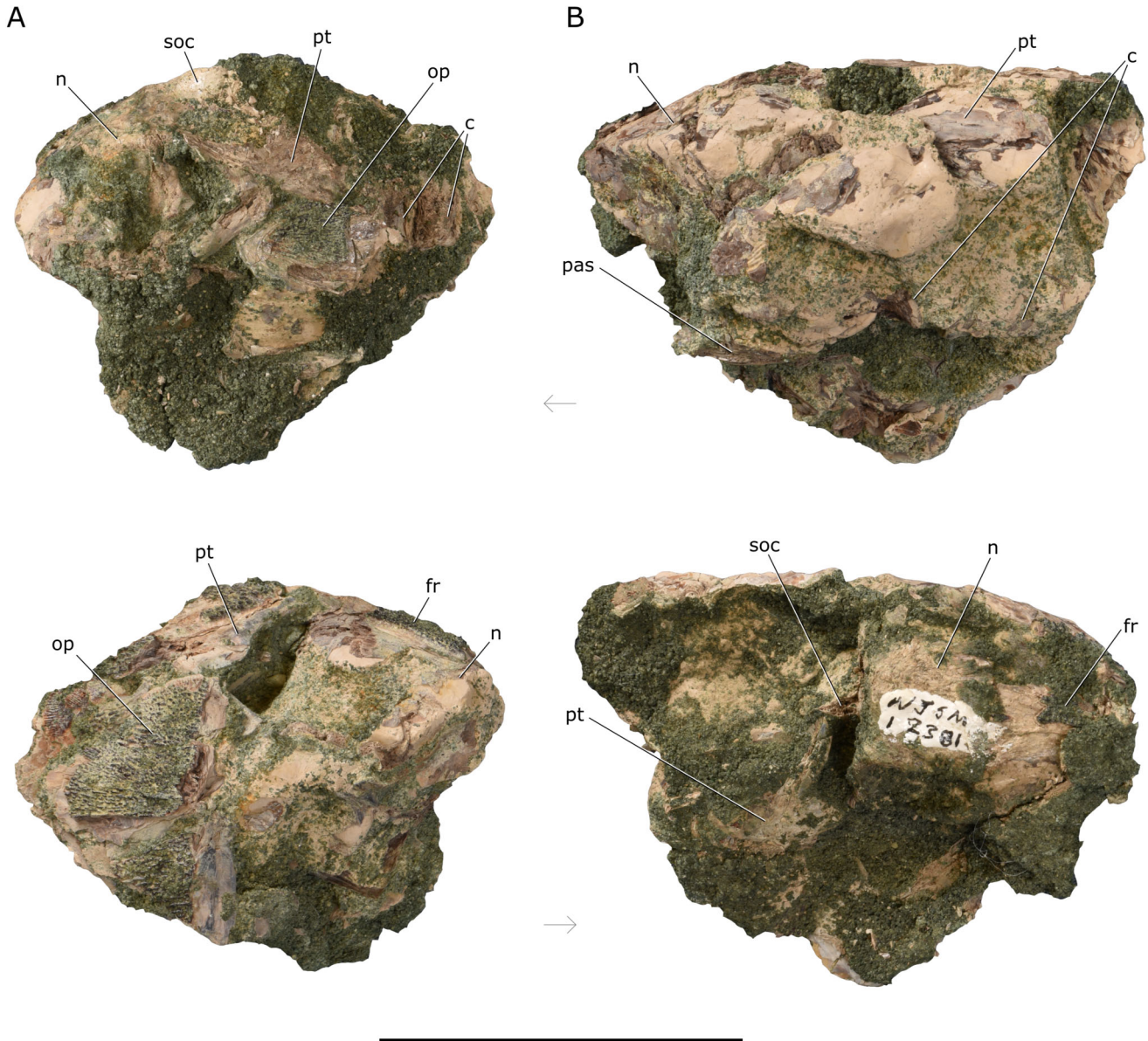


**Figure 5.** Referred specimens of †*Iridopristsis parrisi*. NJSM GP12381, Homerstown Formation, early Paleocene (Danian), New Jersey, USA, comprising remains of two individuals preserving portions of neurocrania, pectoral girdle, opercular series and vertebral column. Upper row depicts the left side of specimens, lower row depicts the right side of specimens. **A**, individual preserving neurocranium including intact supraoccipital crest, fragments of left hyomandibula, right operculum, both posttemporals, and the first three vertebral centra; and **B**, specimen preserving neurocranium including fragmentary supraoccipital crest, right operculum, both posttemporals, and the first three vertebral centra. **Abbreviations:** c, centra; fr, frontal; n, neurocranium; op, opercular; pas, parasphenoid; pt, posttemporal; soc, supraoccipital. Arrows indicate anatomical anterior. Scale bar represents 5 cm.

head of quadrate posterior to orbital margin; an unexpanded otic bulla; an otolith morphology more similar to that found in holocentrine squirrelfishes (heterosulcoid) than the specialized phenotype of myripristine soldierfishes; lack of a dorsally projecting lamina directly anterior to the anguloarticular-quadrate joint on the lateral surface of the anguloarticular; eleven abdominal centra; cycloid scales with spinoid posterior edge.

**Derivation of name.** The prefix of the generic name (*Irido-*) from the Greek genitive declension of *iridis*, meaning ‘rainbow’, and serving as the etymological root for the element iridium. This refers dually to the mosaic nature of characters present in the specimen, and for its occurrence close to the Cretaceous–Palaeogene boundary, known for its famous iridium anomaly (Alvarez et al., 1980). The suffix *-pristis* from the Greek for

‘saw’ (entering zoological usage in this context via Cuvier, 1829), used in the extant holocentrid genera *Myripristis* and *Pristilepis*, and referring to the holocentrid affinity for bearing coarse squamation.

The specific name is in honour of David Parris, Curator Emeritus of Natural History at the New Jersey State Museum, for his discovery of the specimens described here, and in appreciation of his life-long devotion to the study of the North American fossil fauna.

**Material.** Holotype: NJSM GP12145 (Figs 2–4), an articulated skull preserved in three dimensions plus incomplete postcranium. Referred specimens: NJSM GP12381, two isolated neurocrania with associated opercular elements and vertebrae (Fig. 5). Photogrammetric models of the incomplete postcranium and two referred neurocrania can be accessed via Figshare (10.6084/m9.figshare.21754541).

**Occurrence.** ‘Main Fossiliferous Layer’ of the Hornerstown Formation in Sewell, New Jersey, USA.

**Remarks.** NJSM GP12145 is mentioned, but not described, by Stewart (1996), who considered it an intermediate between Cretaceous and Cenozoic taxa. The void space of the saccular otoliths of NJSM GP12145 are figured and described by Schwarzahns *et al.* (2018), who aligned the specimen with holocentrine squarfishes due to an absence of the specialized myripristine otolith morphology described by Schwarzahns (2010).

## Description

**Neurocranium.** The neurocranium of the holotype of †*Iridopristsis parrisi* is broken in two, but remains in association. The anterior portion preserves the mesethmoid, lateral ethmoids, vomer, and part of the parasphenoid, and the posterior portion preserves the frontals, pterosphenoid, parietals, sphenotics, pterotics, epioccipitals, prootics, exoccipitals, basioccipitals, and the remainder of the parasphenoid (Figs 6, 7). The supraoccipital crest, nasals, basisphenoid, and the most lateral portions of the left pterotic are not preserved.

The bones making up the ethmoid region are largely disarticulated, and the nasals are not preserved with the specimen. The mesethmoid is shattered dorsally and is disarticulated from the vomer, while the articulations with the lateral ethmoids are broken but remain in close physical association. The parasphenoid and vomer are articulated, although the vomer is displaced left-laterally. Anterior portions of the frontals that would contribute to the dorsal margin of the orbit are entirely absent. The left frontal is broken anterolaterally where it would contact the supraorbital shelf in life. The left pterosphenoid is broken and displaced mesially. A break

separates the anterior and posterior half of the parasphenoid at the level of the myodome. The posterior portion of the parasphenoid remains tightly bound to the prootic and basioccipital, while the anterior section of the element has been shifted dorsally and to the right. There is no definitive supraoccipital crest preserved in life position on the holotype neurocranium. The midline between the epioccipitals bears a jagged surface and suggests that a laminar, bony extension was broken away at this site. Fragments have been reattached in this area during preparation, but they are incomplete. Instead, description of the supraoccipital crest is based on two referred neurocrania designated NJSM GP12381.

The mesethmoid is best-preserved ventrally, though dorsal pieces are still preserved near the margins of the lateral ethmoids. The mesethmoid is more posterior relative to the vomer than would be expected in life, suggesting taphonomical displacement. The ventral process of the mesethmoid is triangular in ventral view, and would have articulated with the vomer ventrally.

The lateral ethmoids have a broadly triangular aspect in anterior view, and are best-preserved along their lateral margins. The lateral ethmoids are smooth along the orbital margin, with the foramen of the olfactory nerve visible in posterior view, but obscured in anterior view by the shattered mesethmoid.

The vomer is firmly attached to the anteroventral surface of the parasphenoid. A triangular knob emerges from its ventral surface. The dorsal surface of the vomer bears a large lateral flange on either side. Each curves mesially towards its counterpart and the anterior margin of the vomer, forming the notch into which the mesethmoid would have articulated.

The frontals dominate the dorsal surface of the neurocranium. They are ornamented by protuberances arranged in linear series that extend the length of the frontal. These show a radiating pattern, diverging from one another as they approach the posterior margin of the bone. Comparable ornamentation is visible on the referred specimens (Fig. 5; 10.6084/m9.figshare.21754541), representing key evidence supporting their attribution to †*Iridopristsis*. The frontals are triangular in dorsal view, with a deep canal separating them along the midline. The right frontal bears a supraorbital shelf laterally which is ornamented with the same protuberances as the remainder of the frontal. A deep supraorbital canal divides this shelf from the main body of the frontal. Each frontal is divided medially by a canal. The posterior margin of the frontals comprises a ledge that overhangs the most anterior portion of the parietal. The parietals are triangular in dorsal view, and their posterior extremities overhang the epioccipitals.

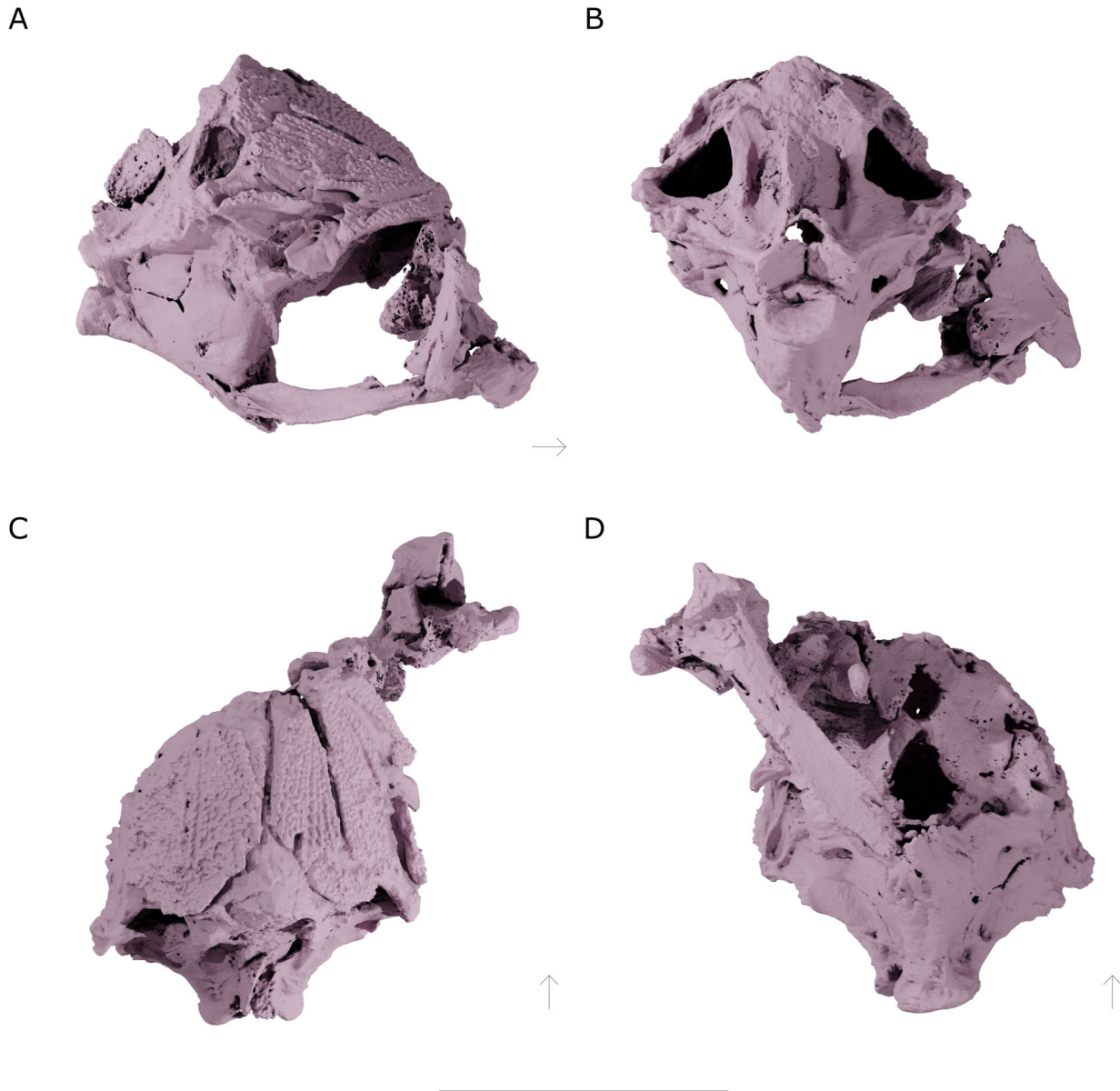


**Figure 6.** Neurocranium of †*Iridopristsis parrisi*. Holotype (NJSM GP12145), Hornerstown Formation, early Paleocene (Danian), New Jersey, USA. Rendered  $\mu$ CT model in **A**, right lateral, **B**, posterior, **C**, dorsal and **D**, ventral views. Arrows indicate anatomical anterior. Scale bar represents 5 cm.

The sphenotic is anterodorsal to the prootic, posteroventral to the frontal, lateral to the pterosphenoid, and anteroventral to the pterotic. It is bounded dorsally by a large lateral flange extending posterolaterally from the margin of the supraorbital shelf towards the exoccipitals. This extension obscures the anterior facet of the hyomandibular head in lateral view. The hyomandibular facet extends across portions of the sphenotic, prootic and pterotic. The pterosphenoid forms the dorsomesial border of the orbit, is bounded dorsomesially by the frontal, dorsolaterally by the sphenotic, the prootic

ventrally, and the other pterosphenoid mesially. The left pterosphenoid appears to be broken away from the remainder of the braincase, but remains in close association.

The pterotic articulates with the epioccipitals postero-mesially, the frontal anteromesially, the sphenotic anteromesially, and the prootic ventrally. The posterior margin of the pterotic comprises the prominent dorsolateral crests on the lateral margins of the skull. The ventrolateral surface of the pterotic bears an articular surface accommodating the posterior head of the

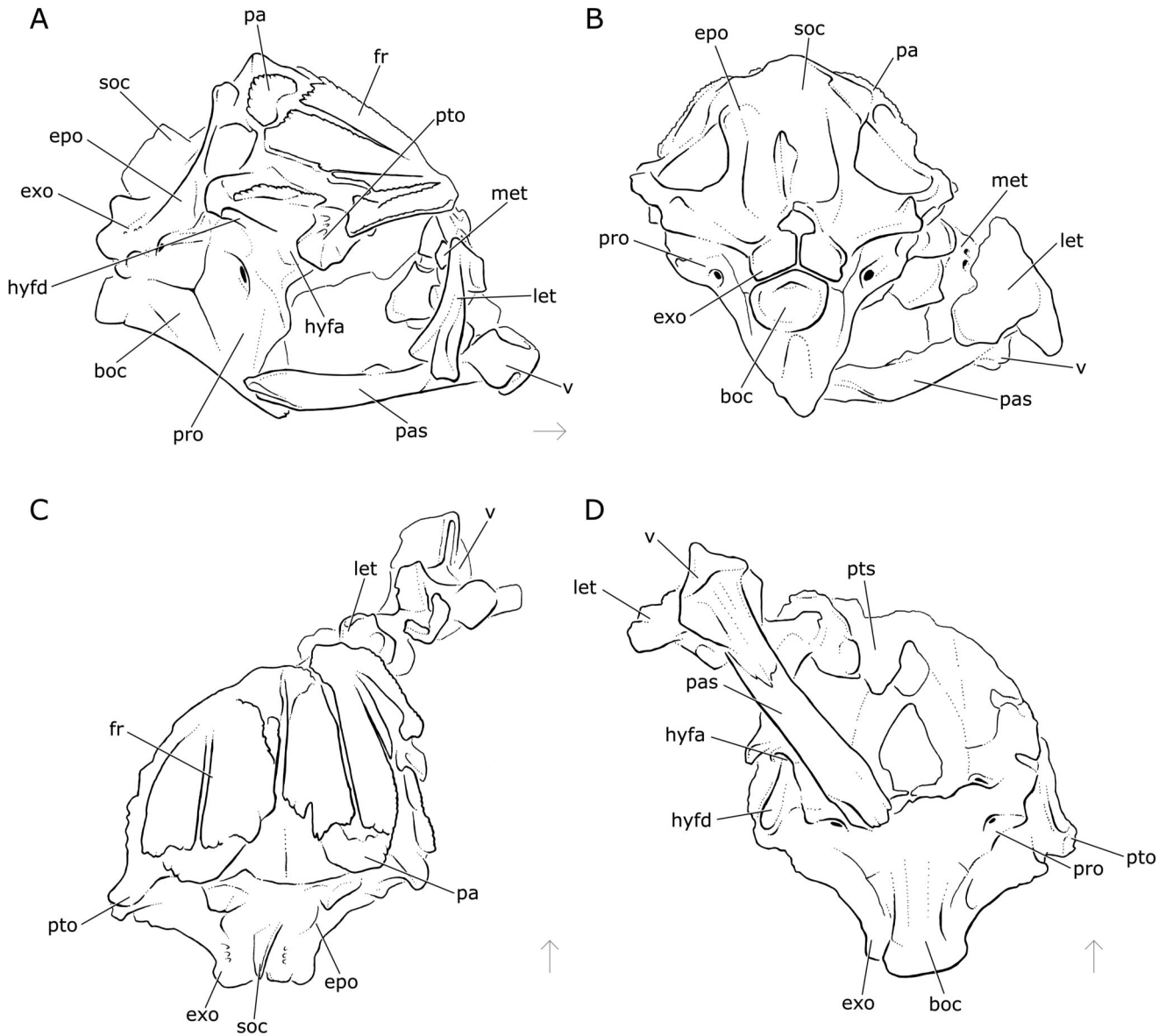


**Figure 7.** Neurocranium of †*Iridopristis parrisi*. Holotype (NJSM GP12145), Homerstown Formation, early Paleocene (Danian), New Jersey, USA. Line drawings of rendered  $\mu$ CT models in **A**, right lateral, **B**, posterior, **C**, dorsal and **D**, ventral views. **Abbreviations:** boc, basioccipital; epo, epioccipital; exo, exoccipital; fr, frontal; hyfa, anterior facet for hyomandibula; hyfd, dorsal facet for hyomandibula; let, lateral ethmoid; met, mesethmoid; pa, parietal; pas, parasphenoid; pro, prootic; pto, pterotic; pts, pterosphenoid; soc, supraoccipital; v, vomer. Arrows indicate anatomical anterior. Scale bar represents 5 cm.

hyomandibula, with the dilatator fossa present on the dorsal surface.

The prootic is bounded by the pterosphenoid anteromedially, the sphenotic anterodorsally, the pterotic dorsally, the exoccipital posterodorsally, the basioccipital posteroventrally, and the parasphenoid ventrally. The prootic carries a dorsoventrally oriented flange lateral to the pars jugularis and posteroventral to the facet for the anterior head of the hyomandibula. The mesial margin

of the prootic is flanged anterolaterally, and forms the dorsolateral margin of the myodome.

The epioccipitals articulate with the pterotic anterolaterally, the parietals and frontals anterodorsally, and the exoccipitals posteroventrally. A buttress along each of the lateral margins of the epioccipital continues ventrally onto the exoccipital. A trough bearing a raised midline extends between these buttresses, marking the presumptive position of the supraoccipital crest.

The referred neurocrania preserve the supraoccipital crest to varying degrees (Fig. 5; 10.6084/m9.figshare.21754541). Together, they suggest that the crest was large and triangular in lateral aspect, being overall more similar to the condition found in myripristines than holocentrines. The supraoccipital is continuous with the dorsal margin of the braincase, extending posteriorly and curving ventrally to form a perpendicular angle with the dorsal margin of the foramen magnum. The dorsal margin of the supraoccipital crest is laterally expanded where it meets the posterior of the braincase; it is not clear if this is a remnant of a transverse crest or if it represents the shape of the supraoccipital itself. The ventral margin of the supraoccipital appears to be in contact with the foramen magnum – a state that has been referred to by other authors as a spina occipitalis (Davesne et al., 2016; Johnson & Patterson, 1993).

The exoccipital is bounded ventrally by the basioccipital, anteriorly by the prootic and pterotic, dorsally by the epioccipital, and mesially by its counterpart. The dorsal portion of the exoccipital bears the ventral continuation of the buttress and trough present on the epioccipital. The lateral margin of the exoccipital forms a prominent shelf that meets the pterotic anteriorly. The most posterior portion of the exoccipital bears a large condyle bounding its counterpart mesially and the basioccipital condyle ventromesially; collectively these form the occipital condyle. Each exoccipital bears three foramina dorsal to the exoccipital condyle, presumably for passage of the occipital nerves (see Patterson, 1964, fig. 48 for homologous foramina in the Cretaceous acanthomorph †*Hoplopteryx lewesiensis* [Mantell, 1822]). The semicircular foramen magnum lies dorsal to the exoccipital condyles.

The basioccipital is bounded dorsally by both exoccipitals, anteriorly by both prootics, and ventrally by the parasphenoid. The basioccipital condyle spans nearly the entire width of both exoccipital condyles. The basioccipital condyle is convex, the margins gently curving dorsally. Along the ventral midline of the occipital condyle is a shallow fossa. Anterior to this fossa is a shallow trough that continues to the boundary of the parasphenoid. These features likely accommodated the soft tissue anatomy of the dorsal aorta in life (see Grande & Bemis, 1998 for examples in fossil amiids).

The lateral wall of the otic chamber is flat, presenting no lateral expansion. Portions of the prootic, exoccipital and basioccipital make roughly equal contributions to this lateral wall. No clear openings in the otic wall are present in the holotype specimen, but the referred neurocrania appear to bear an opening more reminiscent of that piercing the otic bullae of living holocentrids.

The parasphenoid is elongate and contacts the basioccipital posteriorly, the prootic posterodorsally, and the vomer anteriorly. The parasphenoid is approximately triangular in axial cross-section, bearing laterally expanded flanges along the ventral margin posteriorly. There is no mesial ascending process at the level of the myodome that would articulate with the descending process of a basisphenoid. This is interpreted as taphonomical loss rather than genuine absence. The posterior margin of the parasphenoid interdigitates with the ventral surface of the basioccipital, forming small ridges along the posterioventral portion of the neurocranium.

**Infraorbitals and sclerotic ossicles.** The infraorbitals comprise the paired lachrymals (IO1), preserved on both sides of the fossil, and fragments of subocular shelf that are broken away from more posterior infraorbital fragments. No definitive sclerotic ossicles are evident in tomograms. Overall, the infraorbital series is poorly preserved and disarticulated (Figs 2–4).

The left lachrymal is approximately rhomboidal in lateral view, and bears numerous protuberances on the lateral face. Two grooves extend anteroventrally along the lateral surface and are connected to one another beneath a bony bridge. The anteroventral groove spans approximately one-fourth of the total length of the lachrymal, and curves dorsally to meet the more posterior groove. The posterior groove becomes enclosed within the lachrymal at three-fourths the total length of the element, and then re-emerges at the posterodorsal margin. The mesial surface of the lachrymal possesses a posteromesially directed shelf anteriorly emarginated by a dorsoventrally flattened flange. The lachrymal is considerably longer anteroposteriorly than it is tall dorsoventrally.

The more posterior fragments of the infraorbitals are large, approximately square in shape and bear rugose ornamentation on their lateral surfaces. The more mesial fragments of subocular shelf associated with the laterally facing infraorbitals are relatively thick and concave on the orbital margin. Individual bones cannot be identified.

**Jaws.** The upper and lower jaws are preserved in tight association, but are described and figured separately for clarity. The upper jaws consist of the maxillae and premaxillae (Fig. 8A, B). With the exception of the anterior-most quarter of the left example, the supramaxillae are not preserved with the specimen. The ascending process of the premaxillae are not preserved. The shaft of the left maxilla is shattered at multiple points but remains articulated. The descriptions are based on the right upper jaw.

The premaxilla is anteroposteriorly elongate, approximately three-fourths the total length of the maxilla, and

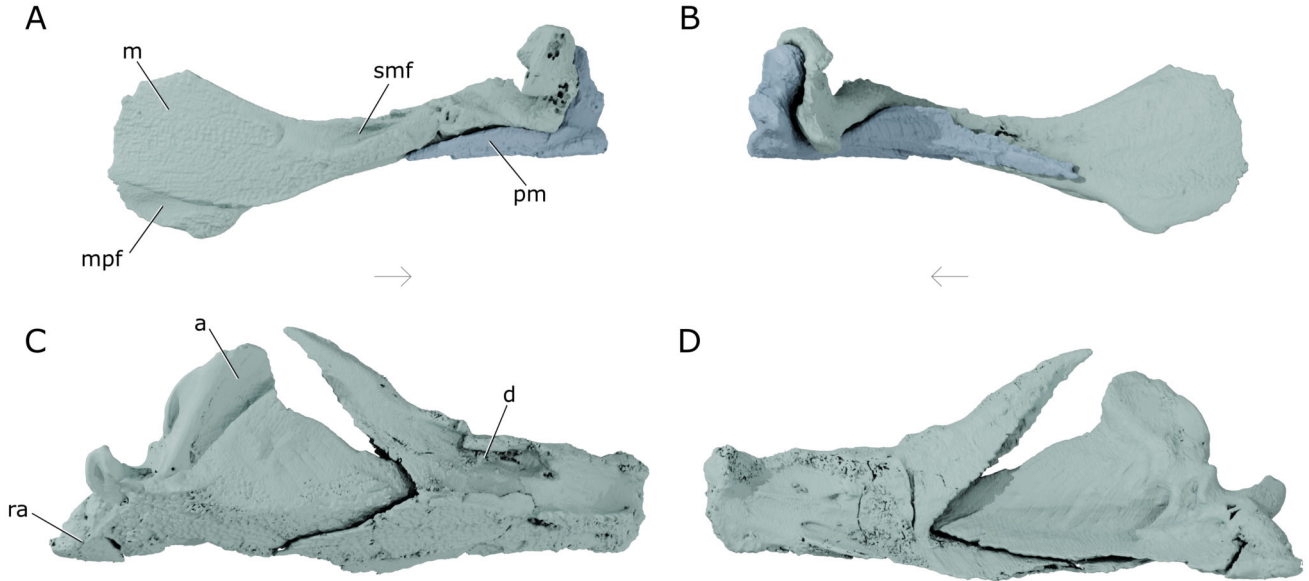


**Figure 8.** Right upper and lower jaws of †*Iridopristsis parrisi*. Holotype (NJSM GP12145), Hornerstown Formation, early Paleocene (Danian), New Jersey, USA. Rendered  $\mu$ CT models of **A**, upper jaw in lateral view (maxilla in light blue, premaxilla in dark blue), **B**, upper jaw in mesial view, **C**, lower jaw in lateral view, and **D**, lower jaw in mesial view. **Abbreviations:** a, anguloarticular; d, dentary; m, maxilla; mpf, posterior facet of maxilla; pm, premaxilla; ra, retroarticular; smf, facet for supramaxillae. Arrows indicate anatomical anterior. Scale bar represents 5 cm.

tightly associated with the maxilla dorsally. The premaxilla comprises an anterior, dorsally projecting articular process closely associated with the head of the maxilla and a more posterior alveolar process that contributes to the oral margin and bears small, rounded teeth. The premaxillary articular process is rounded and oblong in lateral view. What remains of the ascending process is a mesially protruding flange capped dorsally by an irregular surface. As such, the articular process spuriously appears as the dominant feature at the anterior end of the premaxilla. The ventral margin of the ascending process lacks teeth and curves dorsomesially away from the alveolar process, forming an edentulous concavity along the ventromesial margin of the premaxilla. The most anterolateral portion of the alveolar process of the premaxilla is laterally expanded to form a tooth-bearing shelf. The anterior teeth along this shelf are larger and more rounded than those located posteriorly. The alveolar process is deeply grooved dorsally and accommodates the maxilla. The postmaxillary process is approximately twice the height of the underlying alveolar process and elliptical in mesial view, the posterior margin gently sloping down to the rest of the posterior arm. The remainder of the premaxilla is slender and terminates at a point posteriorly.

The maxilla is oar-shaped in lateral view. It lies dorsal to the premaxilla and lateral to the dentary and

angular. The slender anterior portion of the maxilla bears a broad, omega-shaped head. This head covers the posterodorsal margin of the articular process of the premaxilla. A notch posterior to the maxillary head accommodates the anterior process of the palatine. A small rectangular process extends ventrolateral to this groove. The body of the bone posterior to the maxillary head consists of an elongate shaft with an approximately cylindrical cross-section. Small, unorganized protuberances ornament the lateral surface of this shaft. Posterior to the shaft the maxilla becomes laterally compressed and dorsoventrally expanded. This posterior portion is approximately circular in lateral view and bears ornamentation arranged in anteroposteriorly directed rows. A wedge-like facet at the dorsal interface between the maxillary shaft and the posterior expansion marks the articulation area for the supramaxilla(e) (Fig. 8A). The posterior portion of the maxilla bears a triangular, anteriorly directed facet (Fig. 8A, labelled 'mpf') on the ventrolateral margin. This facet aligns with the ventral lamina of the maxilla that articulates with the alveolar process of the premaxilla.

The mandible comprises the dentary, anguloarticular, and retroarticular (Fig. 8C, D). The left anguloarticular is shattered approximately midway along the length, in line with the breaks on the maxillary shaft. Likewise, the posteroventral portions of the left dentary have been

broken and disrupted. Approximately one-quarter of the alveolar platform has broken away midway along the length of the right dentary. Descriptions below are based primarily on the right lower jaw.

In lateral view, the anterior portion of the dentary is rectangular. It bifurcates posteriorly into two tapering processes. The dentary bears larger, more blunt, conical teeth anteriorly than along the remainder of the alveolar platform. These anterior teeth sit on a bulbous region overhanging the most anterolateral margin of the dentary, and align with the mesial edentulous concavity of the premaxilla. Posteriorly, smaller teeth continue along approximately half the length of the dentary. The alveolar platform is broken, but remains articulated in both dentaries. The midlength section of the dentary alveolar platform is bounded ventrally by a deep fossa. A posterodorsally oriented coronoid process lies behind the alveolar platform. This process slopes upwards at approximately  $140^\circ$  and constitutes half the total length of the dentary. The coronoid process rises above the premaxillary alveolar arm, and is mesial to the posterior portion of the maxillary arm. The complementary ventral arm of the dentary and the coronoid process together form a deep posterior socket that accommodates the anterior point of the anguloarticular. The entirety of the ventrolateral surface of the dentary is ornamented by small, anteroposteriorly aligned

protuberances reminiscent of those found on the frontals. Two oblong pores for the mandibular canal are present along this surface, one closer to the anterior margin of the dentary, and another more elongate one at approximately the mid-length of the element.

The anguloarticular inserts into the posterior socket of the dentary, coming to a point anteriorly. The angular bears well-developed condylar and coronoid processes. The latter is laminar and is sinusoidal in transverse cross-section, presumably having accommodated the adductor mandibulae pars rictalis in life (Datovo & Vari, 2013). The ventrolateral surface of the angular is ornamented by the same small, anteroposteriorly directed protuberances found on the dentary and frontals. This ornamentation does not continue onto the retroarticular. The right retroarticular is loosely bound to the right anguloarticular, directly beneath the condylar process. It is approximately triangular in lateral view and, while it is difficult to discern ornamentation on the right retroarticular, the left retroarticular exhibits a reticulated, maze-like pattern not evident on other bones.

**Suspensorium.** The suspensorium comprises the hyomandibula, symplectic, metapterygoid, quadrate, endopterygoid, ectopterygoid, and palatine (Fig. 9A, B).

Descriptions below are based on the better-preserved left side of the specimen.

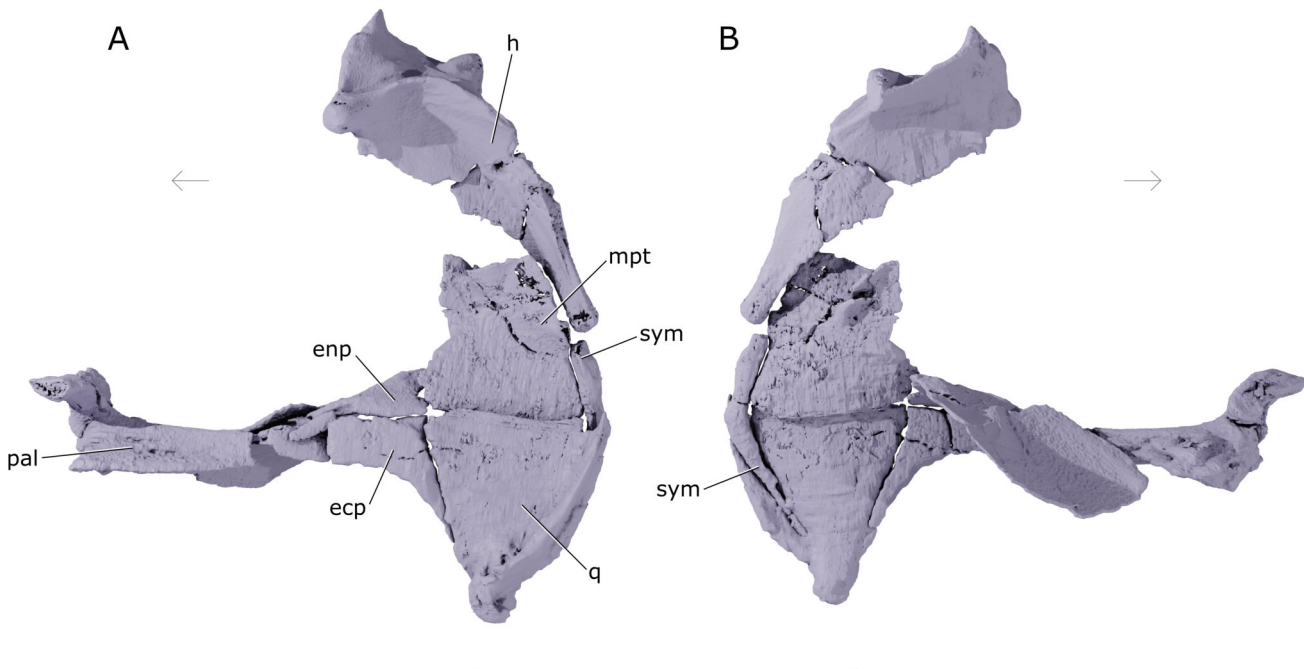


**Figure 9.** Suspensorium of †*Iridopristsis parrisi*. Holotype (NJSM GP12145), Hornerstown Formation, early Paleocene (Danian), New Jersey, USA. Rendered  $\mu$ CT model in **A**, lateral and **B**, mesial views. **Abbreviations:** **ecp**, ectopterygoid; **enp**, endopterygoid; **h**, hyomandibula; **mpt**, metapterygoid; **pal**, palatine; **q**, quadrate; **sym**, symplectic. Arrows indicate anatomical anterior. Scale bar represents 5 cm.



The left hyomandibula is broken at approximately mid-height but remains in life position. The hyomandibula is approximately trapezoidal in lateral view. It is broader dorsally and tapers to a ventral shaft that articulates with the metapterygoid anteriorly and the symplectic and interhyal ventrally. The mesial surface is smooth, but the lateral surface bears a pronounced ridge. This ridge begins one-quarter of the length from the symplectic and interhyal articulation and continues to the height of the opercular process, where it turns anteriorly to meet the rounded dorsal head that joins the suspensorium with the neurocranium. The opercular process of the hyomandibula lies along the same anteroposterior axis as the anterior dorsal head. A dorsally projecting, triangular lamina extends between the dorsal head and the opercular process of the hyomandibula, and is interpreted as a secondary dorsal head. This presumably articulated with the ventral surface of the pterotic in life. Another lamina is present along the ventral margin of the dorsal head of the hyomandibula, bounded dorsally and posteriorly by the pronounced ridge along the dorsoventral midline. The hyomandibular arm terminates ventrally at a head. This ventral head bears an articular surface, two-thirds of which is occupied by the interhyal, with the remainder joining the symplectic.

The left metapterygoid is approximately square in lateral view, with the posterior boundary tightly linked with the ventral arm of the hyomandibula and the symplectic. Ventrally, it joins the dorsal lamina of the quadrate. The most posterodorsal portion of the metapterygoid obscures the hyomandibular shaft in lateral view. The anterodorsal margin of the metapterygoid is bifurcated, bearing a mesially protruding flange anteriorly that is approximately half the total height of the bone.

The quadrate is triangular in lateral view. The posterior margin bears flanges directed posteromesially and posterolaterally, forming a notch on the mesial surface that accommodates the symplectic. A two-headed condyle at the ventral corner of the quadrate articulates with the condylar process of the anguloarticular of the lower jaw.

The symplectic is rod-like and lies in a notch on the inner face of the quadrate. Nearly half the total length of the symplectic extends beyond the dorsal margin of the quadrate, where the bone curves at an angle of approximately 120° to follow the posterior margin of the metapterygoid. The dorsal end of the symplectic articulates with the ventral arm of the hyomandibula. The more ventral portion of the symplectic is thin and tapers to a point, while the dorsal portion is robust with a blunt termination.

The ectopterygoid includes two arms: one that extends anteroposteriorly and one that extends dorsoventrally. The two arms meet at a gentle angle of approximately 100°. The posterodorsal margin comes to a point where the margins of the endopterygoid, quadrate, and metapterygoid meet. The dorsal arm is fractured anteriorly and near the ventral arm, but remains in place. Tomograms show no obvious signs of dentition along the mesial margin of the endopterygoid.

The left endopterygoid is shattered and ventrally displaced. However, it remains in close association with the metapterygoid posteriorly, the palatine anteriorly, and the ectopterygoid ventrally. The lateral surface of the endopterygoid contacts the dorsal surface of the ectopterygoid, and curves mesially to form the thin lamina that defines the floor of the orbital cavity. Dentition is not apparent in tomograms.

The palatine is approximately triangular in coronal cross-section. Its ventral margin bears a laterally protruding, dorsoventrally compressed shelf that extends the length of the bone. The ventrolateral margin of this shelf bears a field of small teeth. A dorsoventrally compressed anterior palatine process attaches to the main body of the palatine at the anterior midline of the bone. The anterior palatine process is strongly turned 45° anterolaterally, wrapping around the dorsal surface of the maxilla and fitting into the groove posterior to the omega-shaped maxillary head. The anterior palatine process is broken from the body of each palatine, but remains in close association.

**Opercular series.** The opercular series comprises the preopercle, interopercle (Fig. 10A, B), and a dissociated operculum separate from the skull portion of the specimen (Fig. 10C, D). No subopercles are associated with the specimen. The right preopercle is not preserved with the specimen, while the left preopercle is broken anteroventrally and shattered posterodorsally, with fragments out of life position. The opercle is only partially intact, with one large fragment, a smaller fragment glued onto the primary fragment, and another small loose piece that is not affixed to the remainder of the element. Descriptions of the opercular series are based on the left side of the skull.

The preopercle is boomerang-shaped in lateral view, with its two arms joining at approximately a 50° angle. The mesial surface bears no notching or ornamentation. The anterior margin of the lateral surface of the preopercle bears a smooth, deep groove that accommodates the ventral arm of the hyomandibula. A ridge located posterior to this smooth surface bears ornament consisting of small protuberances. A broad groove, spanning approximately half the width of the preopercle and floored with smooth bone, lies posterior to this ridge.

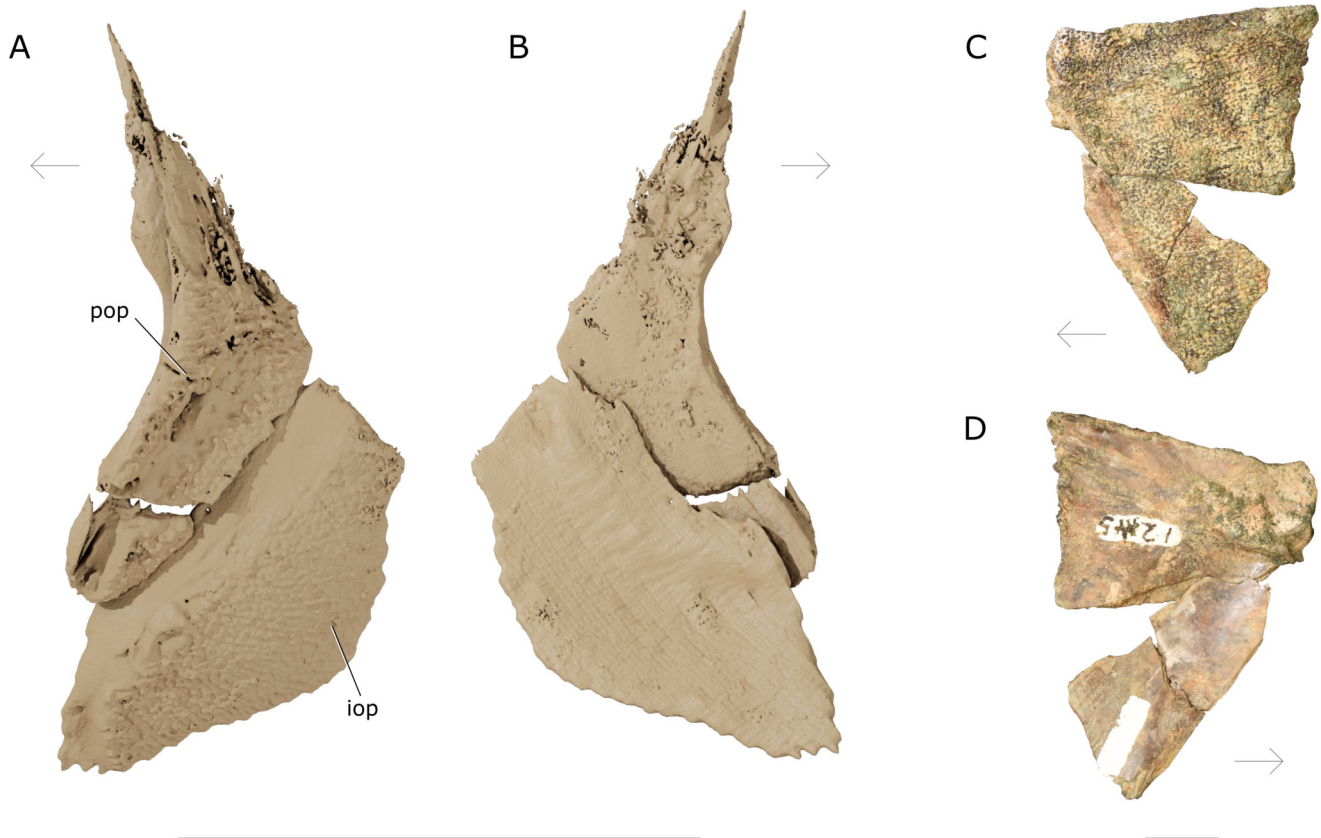


**Figure 10.** Left preopercle and interopercle of †*Iridopristis parrisi*. Holotype (NJSM GP12145), Hornerstown Formation, early Paleocene (Danian), New Jersey, USA. Rendered  $\mu$ CT model in **A**, lateral and **B**, mesial views. Photographs of operculum in **C**, lateral and **D**, mesial views. **Abbreviations:** **iop**, interopercle; **pop**, preopercle. Arrows indicate anatomical anterior. Scale bar represents 5 cm for panels A and B, and 1 cm for panels C and D.

Ornamentation posterior to this groove matches the pattern at the anterior margin of the preopercle.

The interopercle is rhomboidal in lateral view. The mesial surface is smooth. The anterior and dorsal margins bear a smooth surface marking the area of overlap for the preopercle. The ventral portion of the anterior margin, in close association with the anguloarticular, is deeply indented. The remainder of the lateral surface is ornamented in small protuberances.

The operculum bears the opercular facet anteriorly, where it would have met the hyomandibula. The lateral surface bears a lineated rugose ornamentation that is more comparable to the surface texture on the jaws than on other bones of the opercular series (Fig. 10C). A prominent ridge lies along the mesial surface, along the same anteroposterior axis as the opercular facet (Fig. 10D).

**Ventral hyoid arch.** The ventral hyoid arch comprises the dorsal and ventral hypohyals, the anterior and posterior ceratohyals, the branchiostegals, the interhyal, and the urohyal (Fig. 11); it is intact and mostly preserved

in articulation on both sides of the specimen. The urohyal has been displaced away from the basihyal, and the right interhyal is not preserved with the specimen. Many branchiostegals are broken posteriorly, although they remain in association with the ceratohyals anteriorly. Descriptions of the ventral hyoid arch are based on the left side of the skull.

The dorsal hypohyal is approximately rectangular in lateral view, apart from a notch-like canal at the middle of its ventral margin. The ventral hypohyal has a rounded anterior margin and bears a posteroventral facet that articulates with the anterior head of the anterior ceratohyal. The remainder of the posterior margin of the ventral hypohyal curves posterodorsally with the articular surface of the anterior ceratohyal.

The anterior ceratohyal is laterally compressed and approximately trapezoidal in lateral dimension. Its anterior margin slopes down to an anterior head that meets the ventral hypohyal. The ventral margin bears four notches marking articulations for branchiostegals. The posteroventral corner of the anterior ceratohyal is broken and displaced mesially. The posterior margin of the anterior

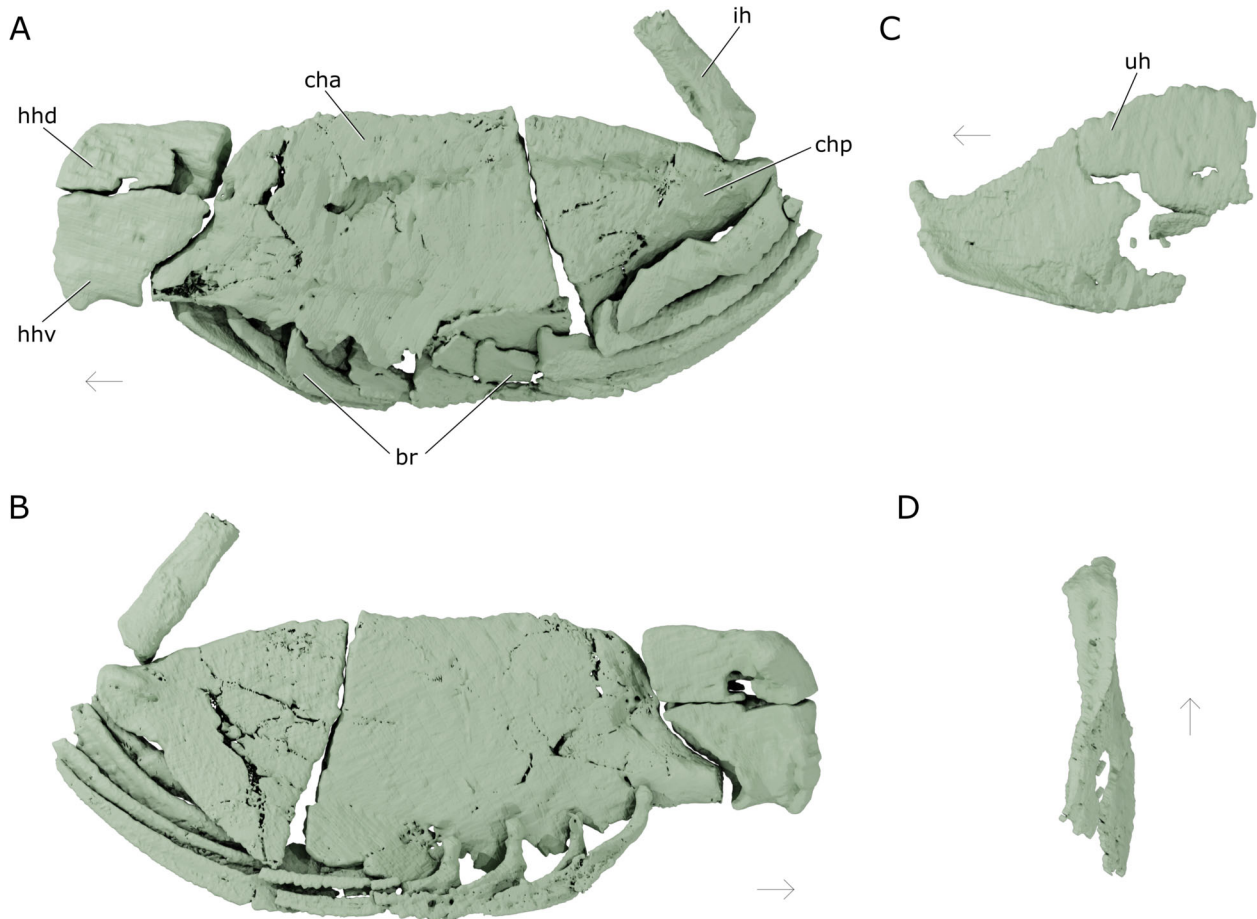


**Figure 11.** Left ventral hyoid apparatus of †*Iridopristis parisi*. Holotype (NJSM GP12145), Homerstown Formation, early Paleocene (Danian), New Jersey, USA. Rendered  $\mu$ CT models showing the **A**, lateral and **B**, mesial views of the hypohyals, ceratohyals, interhyal, and branchiostegals, and the **C**, urohyal in lateral and **D**, ventral view. **Abbreviations:** **br**, branchiostegals; **cha**, anterior ceratohyal; **chp**, posterior ceratohyal; **hhd**, dorsal hypohyal; **hhv**, ventral hypohyal; **ih**, interhyal; **uh**, urohyal. Arrows indicate anatomical anterior. Scale bar represents 5 cm.

ceratohyal is flush with the posterior ceratohyal, and bears no evidence of fusion to the latter. The anterior ceratohyal is imperforate, instead bearing a deep groove on the lateral surface extending two-thirds the length of the bone and continuing onto the posterior ceratohyal.

The posterior ceratohyal is triangular in lateral view and laterally compressed. The anterior margin is straight and meets the anterior ceratohyal. A thickened knob at the posterior tip of the posterior ceratohyal marks the articular surface for the interhyal. The interhyal is an oblong rectangle in lateral view. Its ventral tip contacts the posterior ceratohyal. The interhyal bears a deep fossa along the ventrolateral margin that is directed anterodorsally from the articulation with the ventral facet.

Four branchiostegals articulate with the ventral margin of the anterior ceratohyal, while an additional three branchiostegals lie lateral to the anterior ceratohyal and

another two lie lateral to the posterior ceratohyal. The four branchiostegals that articulate with the ventral margin of anterior ceratohyal bear pronounced hook-like processes at their proximal ends. More posterior branchiostegals bear weaker hooks. The branchiostegals protrude laterally along the midline of the anteroposterior axis, a feature mirrored by a shallow groove along the mesial surface, defining a chevron-like shape in transverse cross-section. The ventral margin of the branchiostegals do not bear any visible spination.

The urohyal is shattered posteriorly. It is approximately triangular in lateral view (Fig. 11C) and bears an anteriorly directed dorsal ramus. Lateral flanges extend from the ventral margin of the urohyal, and taper posteriorly. These flanges form a ventrally directed midline pocket, the inside of which bears four visible notches (Fig. 11D).

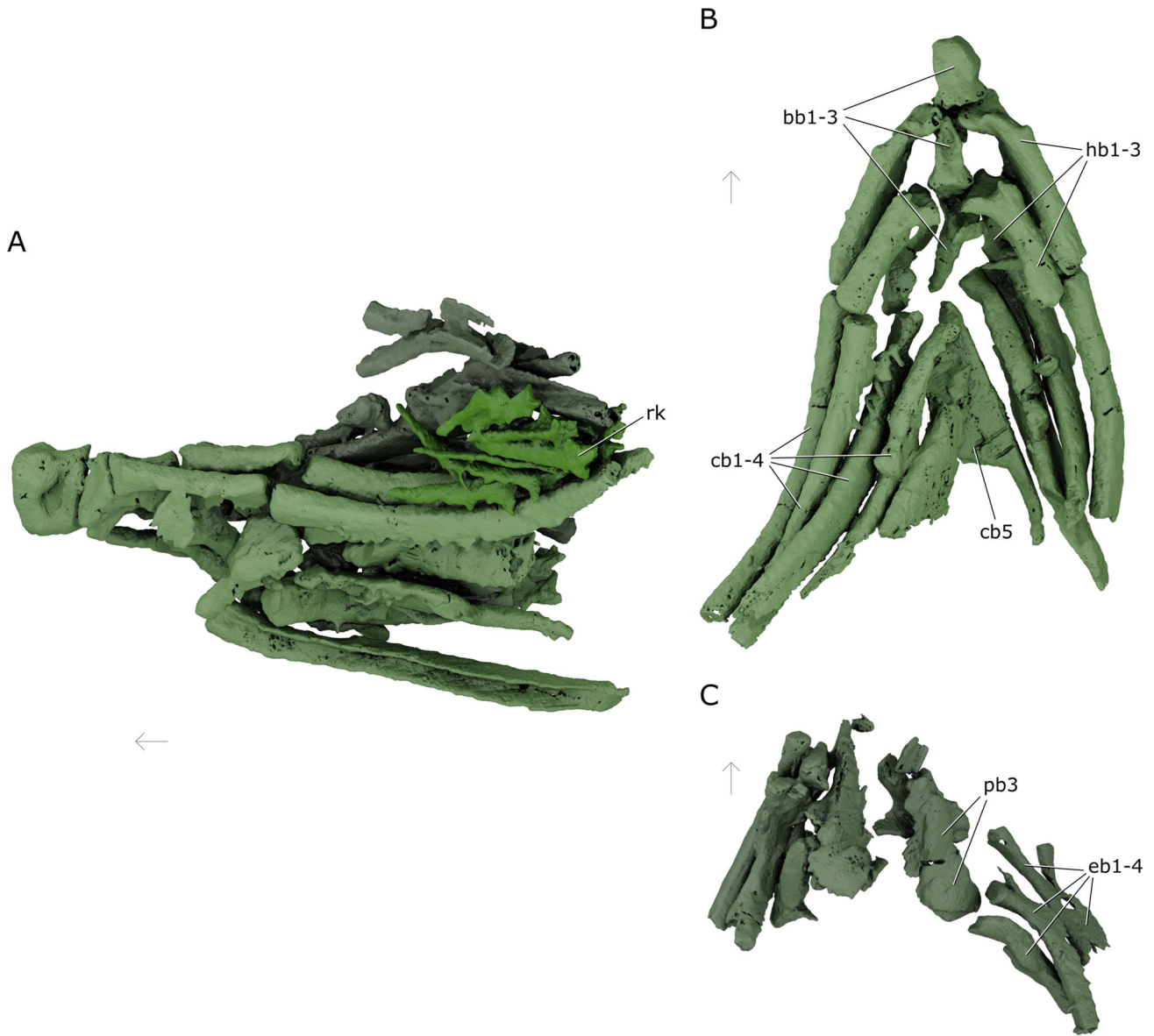


**Figure 12.** Gill skeleton of †*Iridopristis parrisi*. Holotype (NJSM GP12145), Hornerstown Formation, early Paleocene (Danian), New Jersey, USA. Rendered  $\mu$ CT models of **A**, complete gill skeleton in lateral view, including the dorsal and ventral gill skeleton and associated gill rakers, **B**, ventral gill skeleton in dorsal view, **C**, dorsal gill skeleton in ventral view. Ventral gill skeleton in green, dorsal gill skeleton in olive, gill rakers in lime. **Abbreviations:** **bb**, basibranchials; **cb**, ceratobranchials; **eb**, epibranchials; **hb**, hypobranchials; **pb**, pharyngobranchials; **rk**, gill rakers. Arrows indicate anatomical anterior. Scale bar represents 5 cm.

**Ventral gill skeleton.** The ventral gill skeleton comprises basibranchials 1–3, hypobranchials 1–3 and ceratobranchials 1–5 (Fig. 12A, B). The ventral gill skeleton is articulated anteriorly and laterally, while the more posterior and mesial portions are more disrupted. There is no evidence of the basihyal in tomogram slices; similarly, basibranchial 4 and hypobranchial 4 cannot be seen or are not readily identifiable in the specimen. Descriptions of the ventral gill skeleton are based on

whichever branchial bones are most identifiable rather than those from one side of the specimen.

Basibranchial 1 is short and knob-like, rounded and thicker anteriorly, tapering posteriorly where it meets basibranchial 2 and hypobranchial 1. Basibranchial 2 is more elongate than basibranchial 1, and bears an antero-ventral arm that is associated with the posterior margin of basibranchial 1. Basibranchial 3 is taphonomically shifted ventrally and to the right, and is thickened

anteriorly where it meets basibranchial 2. Posteriorly it tapers to a point.

Hypobranchial 1 is elongate and linear, with an anterior head thinner in transverse cross-section than the remainder of hypobranchial 1 and curving ventromedially to meet the basibranchials. Hypobranchial 2 is shorter than hypobranchial 1 and similarly possesses an enlarged anterior head that curves mesially towards the interface of basibranchial 2 and basibranchial 3. The ventral surface of hypobranchial 2 is hollowed.

Ceratobranchial 1 is rod-like. Its dorsal surface is smooth, while its ventral surface is hollowed out, bearing lateral laminae that enclose a longitudinal trough which would have accommodated the gill filaments in life. Ceratobranchials 2–4 are broadly similar to CB1. The right ceratobranchial 5 is rod-like, bearing a diamond-shaped platform on the dorsal surface that spans three fourths the total length.

Tomograms do not reveal any visible pharyngeal teeth.

**Dorsal gill skeleton.** The dorsal gill skeleton comprises epibranchials 1–4 and pharyngobranchial 3 as a toothplate (Fig. 12A, C). The dorsal gill skeleton is greatly disrupted from life position on the right side of the skull. The left side is more intact, remaining in partial association with the ventral gill skeleton. All descriptions of the dorsal gill skeleton are based on the left side members.

Epibranchial 1 is elongate and bears a dorsal groove beginning at the posterior margin and spanning half of the total length. This groove terminates at an anterodorsally facing uncinat process approximately one-third the total length of epibranchial 1. Epibranchial 2 is approximately the same length of epibranchial 1 and bears a dorsal groove that terminates posteriorly, extending approximately three-fourths the total length of the element. The mesial margin of this groove bears a lamina that forms part of a broad anterior head that would articulate with the pharyngobranchials in life. Epibranchial 3 is approximately two-thirds the lengths of epibranchials 1 and 2. Epibranchial 3 is elongate and bears a dorsal groove extending two-thirds the length of the surface. A large uncinat process approximately one-third the overall length of the bone projects dorsally from the middle of the mesial face of epibranchial 3. The posterior margin of the uncinat process of epibranchial 3 bears a thin lamina that extends half the length to the posterior margin. Epibranchial 4 is more expanded at its proximal and distal ends than at its mid-length, where it bears a large uncinat process.

Pharyngobranchial 3 is roughly triangular in ventral view, and forms a continuous pharyngeal tooth plate ventrally, though a small taphonomical break separates

the anterior and posterior portions of the element. There is a posterodorsally directed process on the dorsal surface approximately midlength along the lateral margin of pharyngobranchial 3. As in extant holocentrids, there does not appear to be a pharyngobranchial 4.

**Gill rakers.** Approximately six gill rakers are preserved in association with the first gill arch (Fig. 12A). These are elongate, roughly one-third of the total length of ceratobranchial 1. They are cruciform, with a small head proximally, two points branching perpendicular to the main axis, and converging to a point distally.

**Pectoral girdle.** Preserved portions of the pectoral girdle include the most dorsal portions of the left supracleithrum and cleithrum, the ventral portion of postcleithrum 1, the dorsal portion of postcleithrum 2, fragmentary portions of the right cleithrum, and the most ventral portions of the cleithrum on both sides of the specimen (Fig. 13). The entirety of the pectoral girdle is fragmentary. Descriptions of the supracleithrum, cleithrum and postcleithrum are based on the left-side members.

The fragment of the supracleithrum is lateral to the most dorsal piece of the cleithrum, and is approximately triangular in shape. The anterior margin of the cleithrum is nearly vertical, while the posterior margin is approximately semicircular. The postcleithrum lies mesial and ventral to the cleithrum. Postcleithrum 1 is broken dorsally, appearing almost rectangular in lateral aspect. The anterior margin is roughly straight, while the posterior margin is rounded off. The fragmentary piece of postcleithrum 2 is approximately triangular.

The ventral portion of the cleithrum is shattered but individual fragments remain in close association. It is weakly sinusoidal in dorsoventral cross-section, and follows the posterior margin of the skull from the edge of the opercles to the midline. Mesially, the ventral portion of the cleithrum is curved posteriorly to associate with its counterpart.

**Pelvic girdle.** There are no fragments of pelvic girdle preserved in the holotype or referred material.

**Squamation.** Cycloid scales with a spinoid posterior margin are present along the entirety of the holotype specimen (Fig. 14). These scales are ovoid, with a height greater than their width. On the skull, scales can be found lateral to the quadrate and metapterygoid, between the posterior margin of the maxilla and the anterior margin of the preopercle, and along the ventral surface between the angular and subopercle (Fig. 14A). The scales on the cheek have approximately 20 pronounced, anteroposteriorly-aligned ridges. Anteriorly, the ridges of the cheek scales coalesce to form a reticulated pattern. The scales on the ventral surface of the

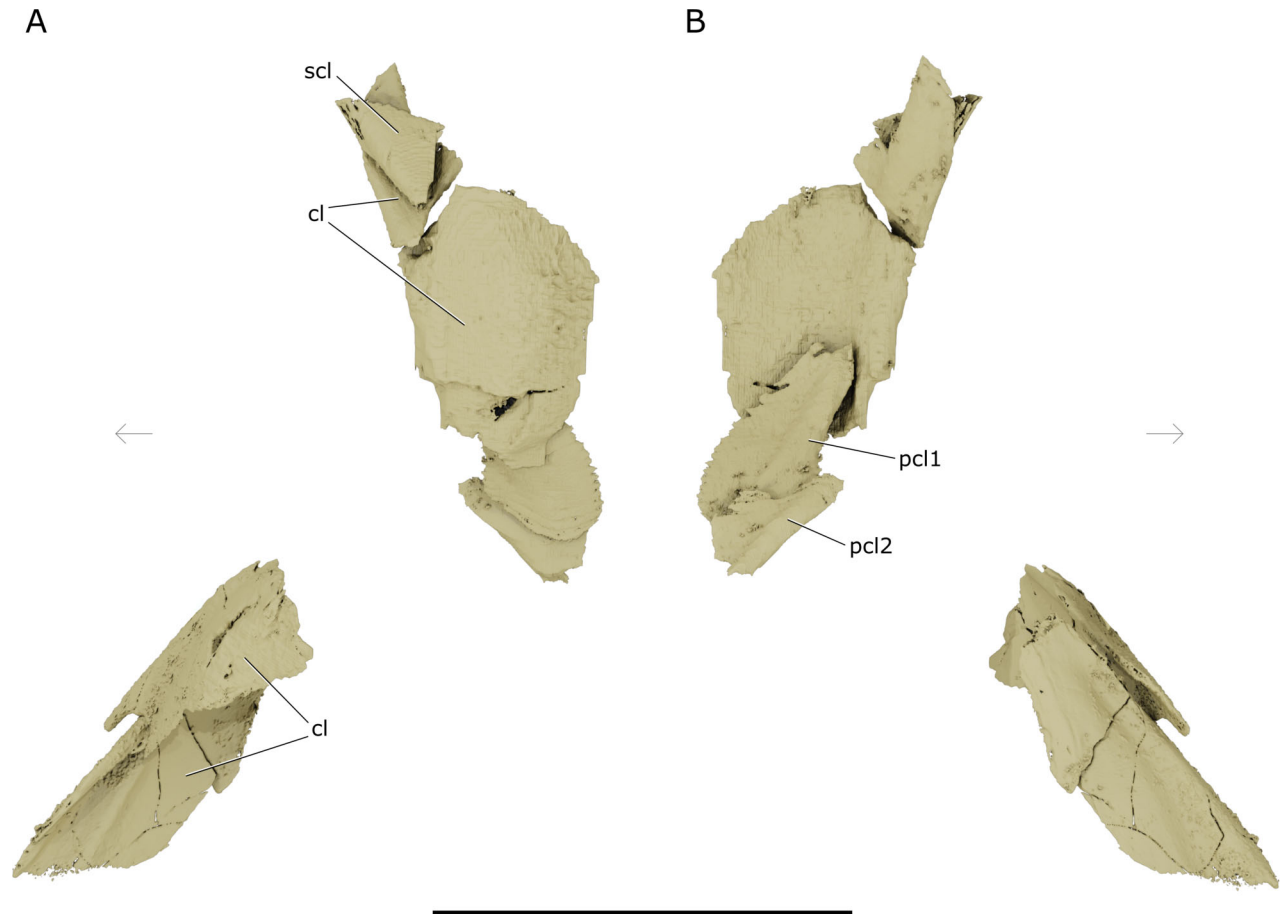


**Figure 13.** Pectoral girdle of †*Iridopristis parrisi*. Holotype (NJSM GP12145), Hornerstown Formation, early Paleocene (Danian), New Jersey, USA. Rendered  $\mu$ CT model in **A**, left lateral and **B**, right lateral views. **Abbreviations:** **cl**, cleithrum; **co**, coracoid; **pcl**, postcleithrum; **scl**, supracleithrum. Arrows indicate anatomical anterior. Scale bar represents 5 cm.

skull specimen bear fewer spines at the posterior margin than those on the cheek. The abdomen is covered in scales larger than those on the head (Fig. 14B). Spination is numerous, with greater than 25 ridges along the posterior margins of each scale, though these ridges are less well developed than those of the cheek scales. Each scale along the lateral line bears a large anteroposteriorly aligned crest, with a pore at the posterior margin of the anterior overlapping scale. The lateral line aligns approximately with the height of the vertebral column for the length of the preserved abdomen.

**Axial skeleton.** The articulated postcranium of the holotype preserves 13 vertebrae in total: a complete series of 11 abdominal vertebrae plus the two anterior-most caudal vertebrae (Fig. 15). The first centrum lacks a preserved neural arch or evidence of a broken neural arch, and it is interpreted as being autogenous as in extant holocentrids. The remaining neural arches are broken and not diagnostic. Two small, rod-like epineurals are present anteriorly. The first three centra bear strongly developed transverse

processes, while the transverse processes of centra 4 and 5 are weakly developed. The remaining centra do not appear to bear transverse processes. Ribs begin on the third centrum, and appear to be taphonomically absent from centra 8–10. The 11th centrum bears a fragment of the final rib that may be antero-posteriorly expanded as in extant berycids and holocentrids. Centra 7–11 bear ventrally directed parapophyses to which ribs would have articulated; these processes increase conspicuously in length along the series. A bridge between parapophyses on centrum 9 encloses an aortic canal, and subsequent centra bear the canal. Haemal spines begin on the 12th centrum, and are inclined posteriorly.

## Results

### New characters bearing on holocentroid phylogeny

In the course of describing †*Iridopristis* and reviewing the anatomy of other berycimorph fishes, we identified

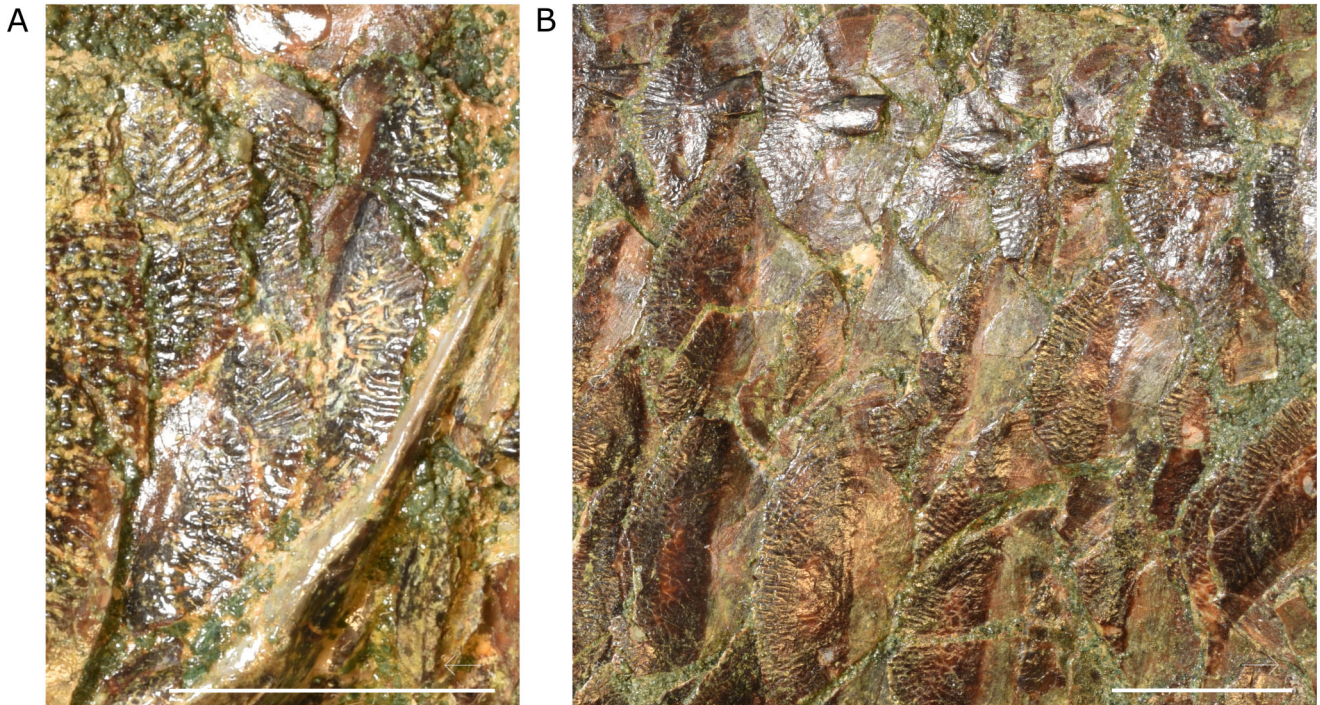


**Figure 14.** Squamation of †*Iridopristis parrisi*. Holotype (NJSM GP12145), Hornerstown Formation, early Paleocene (Danian), New Jersey, USA. Photographs of the **A**, cheek and **B**, abdominal squamation. Arrows indicate anatomical anterior. Scale bars represent 1 cm.

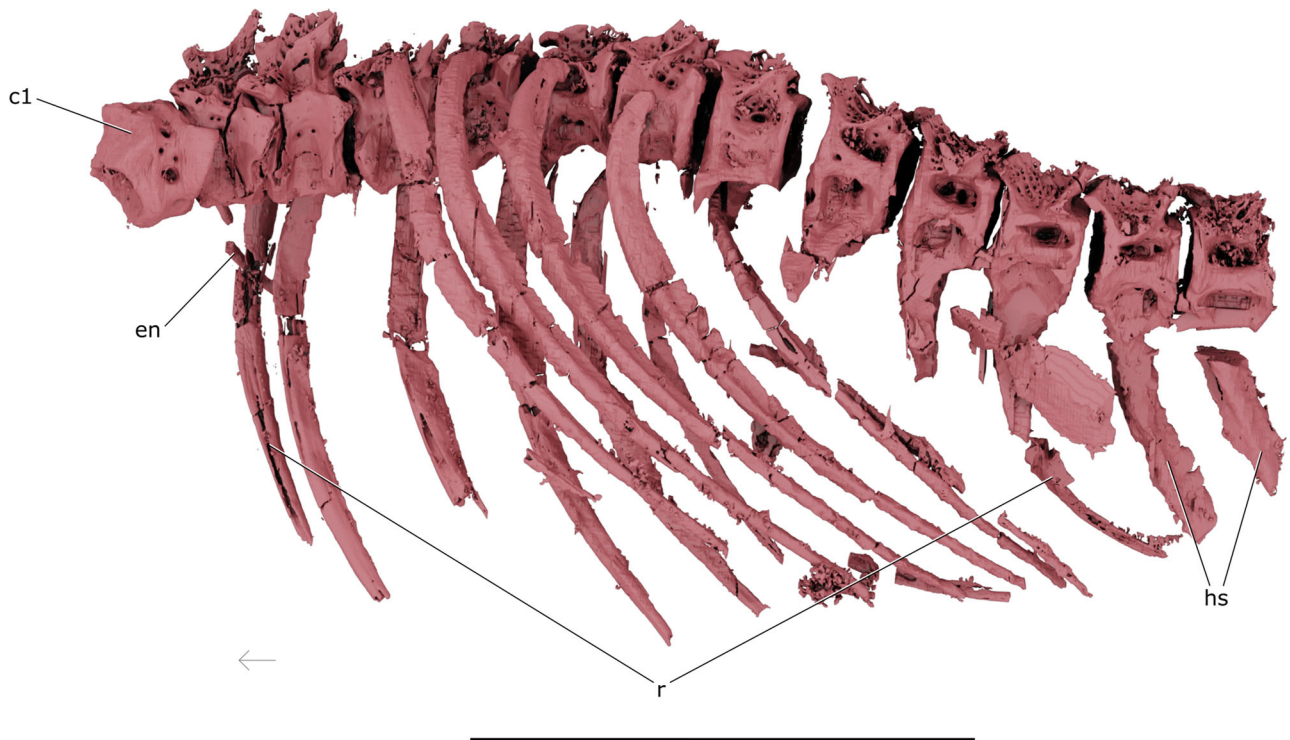


**Figure 15.** Axial skeleton of †*Iridopristis parrisi*. Holotype (NJSM GP12145), Hornerstown Formation, early Paleocene (Danian), New Jersey, USA. Shown in left lateral view. **Abbreviations:** **c**, centra; **en**, epineural; **hs**, haemal spines; **r**, ribs. Arrow indicates anatomical anterior. Scale bar represents 5 cm.

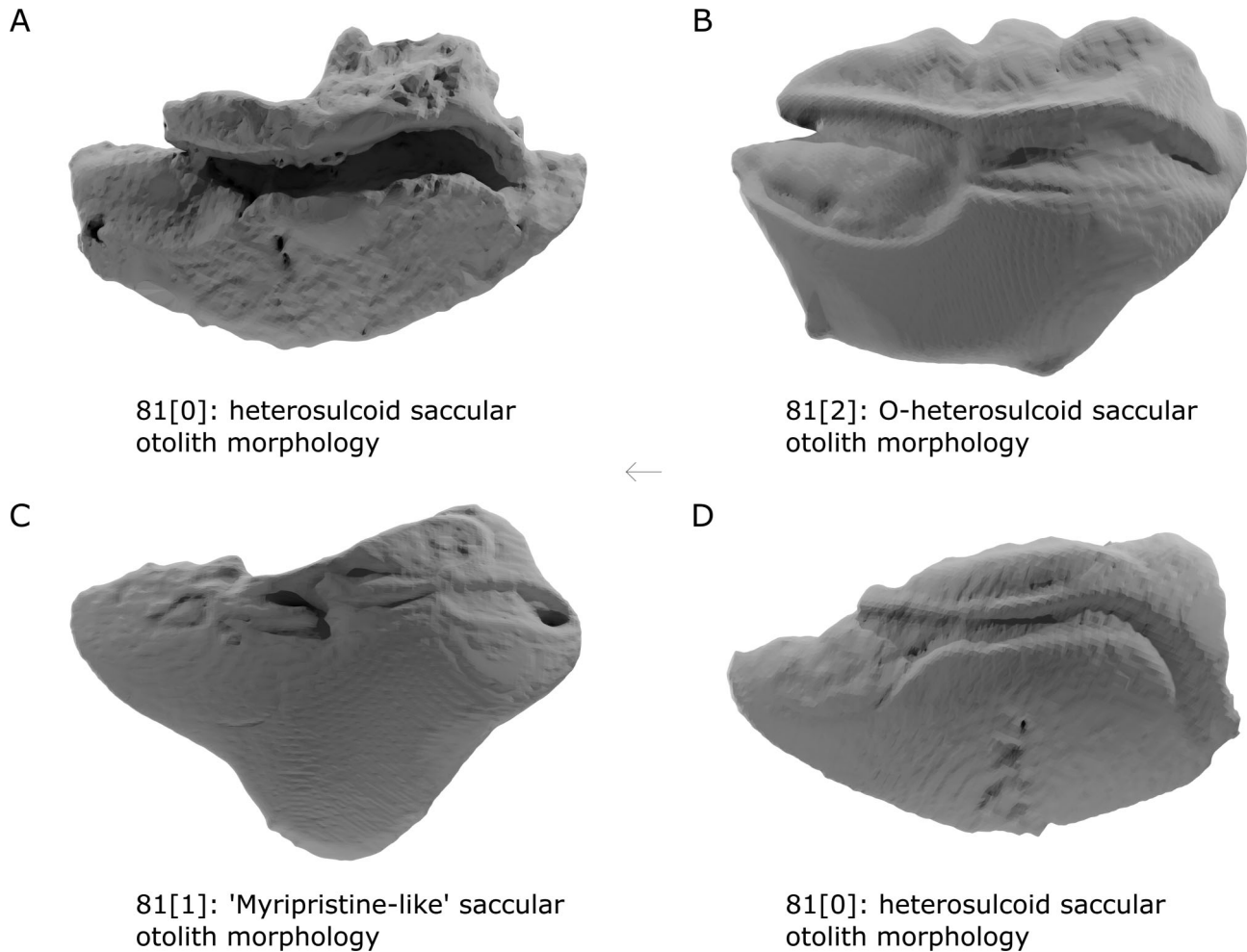


**Figure 16.** Variation in saccular otolith morphology among holocentroids and outgroups. Rendered  $\mu$ CT models of saccular otoliths as a visual explanation of states in Character 81 for **A**, †*Iridopristis parrisi* (NJSM 12145), **B**, *Centroberyx affinis* (UMMZ 216732), **C**, *Myripristis murdjan* (UMMZ 185696), and **D**, *Sargocentron rubrum* (UMMZ 245614). Arrow indicates anatomical anterior. Images not to scale.

two additional characters of possible systematic relevance (Figs 16, 17). We added these characters to our matrix and discuss them in detail here.

**Character 81.** Shape of saccular otoliths. (0) Heterosulcoid otolith morphology (*sensu* Schwarzhans, 1978; Schwarzhans et al., 2017) present in *Polymixia*, holocentroid subclade Holocentrinae (Fig. 16D), and †*Iridopristis* (Fig. 16A), and is the predominant phenotype present in percomorphs. (1) *Myripristis*-like otolith morphology as described by Hecht (1982) and Schwarzhans (2010), with no rostrum, excisura or antirostrum, and a sulcus bounding the dorsomesial margin, occasionally bearing undulatory patterning along the dorsal portion of the sulcus (as in *Myripristis*) present in holocentroid subclade Myripristinae (Fig. 16C). (2) ‘O-heterosulcoid’ otolith morphology (‘archaesulcoid’ of Schwarzhans et al.,

2017) present in *Beryx* and *Hoplostethus* in the matrix, representing the generalized ‘berycimorph’ shape (Fig. 16B) common outside of Holocentridae. Gross otolith morphology can broadly capture taxonomical and functional diversity (Reichenbacher et al., 2007; Tuset et al., 2016), suggesting that it can be a useful predictor of phylogenetic relatedness. Here, we put forth that incorporating this character and the associated character states would be of use in inferring phylogenetic relationships. Fossils bearing *in situ* otoliths are rare (Schwarzhans et al., 2018), and none of the comparative fossil material examined possessed preserved otoliths. As such, with the exception of †*Iridopristis parrisi*, this character was only scored for extant taxa. †*Iridopristis parrisi* shows state 0 for this character, which was used by previous authors to suggest an affinity with the holocentroid subclade Holocentrinae (Schwarzhans et al., 2018).



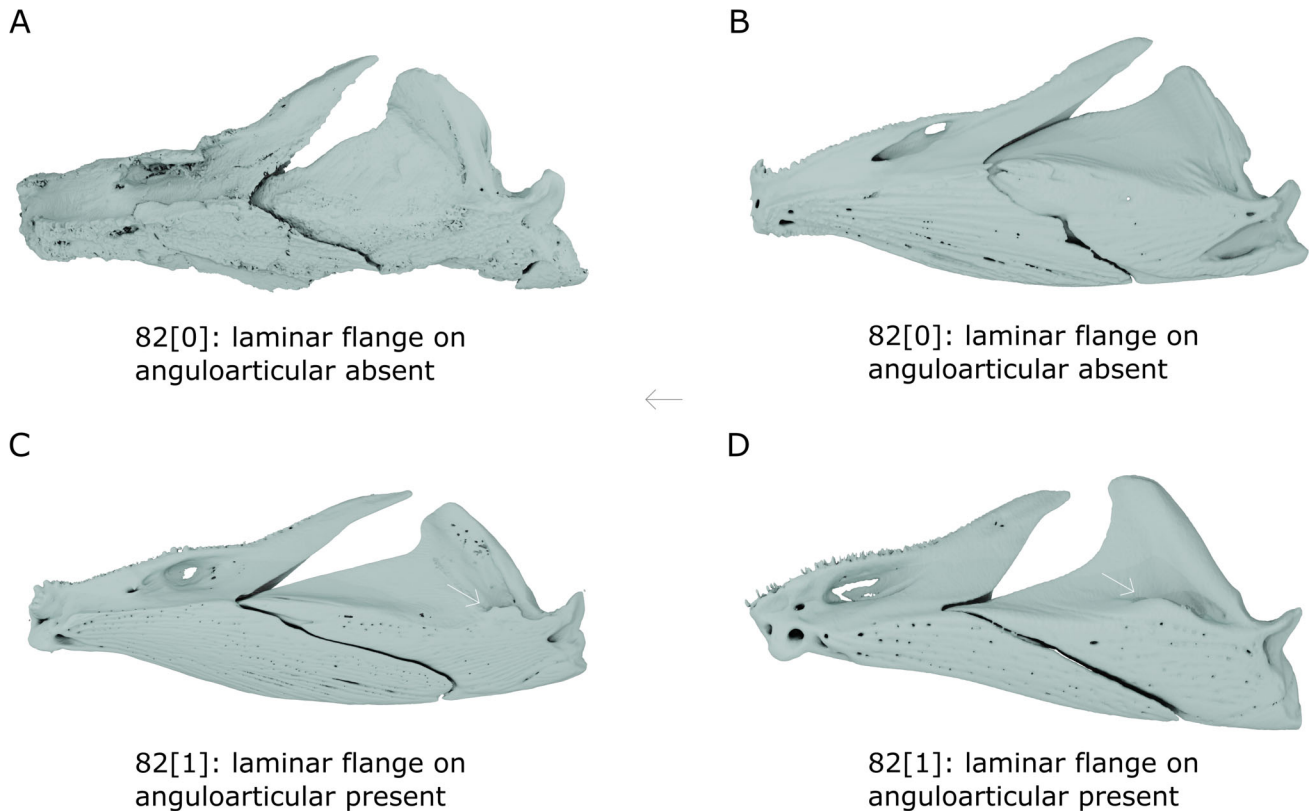


**Figure 17.** Variation in anguloarticular morphology in holocentroids and outgroups. Rendered  $\mu$ CT models of lower jaws as a visual explanation of character states in Character 82 for **A**,  $\dagger$ *Iridopristis parrisi* (NJSM 12145), **B**,  $\dagger$ *Centroberyx affinis* (UMMZ 216732), **C**, *Myripristis murdjan* (UMMZ 185696), and **D**, *Sargocentron rubrum* (UMMZ 245614). White arrows in (C) and (D) indicate laminar flange anterior to jaw joint. Central arrow indicates anatomical anterior. Images not to scale.

**Character 82.** Laminar flange directed dorsally on the lateral surface of the anguloarticular, immediately anterior to the anguloarticular-quadrato joint. (0) Absent (Fig. 17A, B). (1) Present (Fig. 17C, D). The flange referenced by this character lies at the postero-ventral base of the coronoid process, and may serve as an attachment site for the preangular ligament based on its attachment location in other fishes (Datovo & Vari, 2013). Crown-group holocentrids from both subclades (Holocentrinae and Myripristinae) possess this flange, though one specimen of *Plectrypops lima* (UMMZ 185889) lacks it. In all of these examples, the lower-most cheek scale slotted into the gap between the main body of the anguloarticular and the lamina. The character is absent in examined specimens belonging to Berycidae, Melamphaidae, Monocentridae and Trachichthyidae.  $\dagger$ *Iridopristis parrisi* and  $\dagger$ *Caproberyx* also lack this flange, but it is present in  $\dagger$ *Berybolcensis*. It was not possible to score this character other fossils, including  $\dagger$ *Tenuicentrum* and  $\dagger$ *Eoholocentrum*, given preservation or inability to discern state given material available.

### Phylogenetic analysis

**Parsimony analyses.** A parsimony analysis recovers 588 most parsimonious trees of 112 steps. The strict consensus of these trees is poorly resolved (Fig. 18A). All holocentroids, with the exception of the putative member  $\dagger$ *Caproberyx*, fall within a large polytomy. *Beryx* is the sister lineage to this holocentroid clade. Within holocentroids, the only subclades resolved are (1) a sister-lineage pair of  $\dagger$ *Tenuicentrum* plus  $\dagger$ *Berybolcensis*; and (2) a clade of extant holocentrines (*Neoniphon*, *Sargocentron* and *Holocentrus*) plus  $\dagger$ *Eoholocentrum* on its stem. The holocentroid total group and extant holocentrines represent the most robustly supported clades in the tree, both with a Bremer decay index of 5 and bootstrap support of at least 90%.

The agreement subtree generated in PAUP (Fig. 18B) finds the following fossil taxa to be acting as phylogenetic rogues within the analysis:  $\dagger$ *Caproberyx*,  $\dagger$ *Tenuicentrum*,  $\dagger$ *Berybolcensis*,  $\dagger$ *Holocentrites ovalis* Conrad, 1941 and  $\dagger$ *Africentrum melitense* (Woodward, 1887). The agreement subtree shows two important

features agreed upon by the set of most parsimonious trees, but obscured by unstable taxa in the strict consensus: (1) the monophyly of extant myripristines (*Myripristis*, *Ostichthys*, *Pristilepis*, *Plectrypops* and *Corniger*); and (2) placement of †*Iridopristsis* as sister to holocentrids, on the stem of the extant radiation.

**Fossilized birth–death analysis.** The Bayesian analysis expands upon the basic parsimony analysis by sampling additional extant lineages, as well as including molecular and stratigraphical data. In addition to inferring patterns of relationships, it further provides an estimate of divergence times between sampled lineages.

The Bayesian topology is reasonably well resolved, with a majority of nodes having posterior probabilities approaching 1. The greatest topological uncertainties typically relate to nodes subtending one or more fossil lineages; several of these nodes are unresolved. However, clade membership at the broadest level is well supported for most fossil holocentroids included in the analysis. Holocentrines and myripristines are reciprocally monophyletic. As in the parsimony analysis, †*Eoholocentrum* is a stem holocentrine. †*Holocentrites* and †*Africentrum* are myripristines, resolved on the stem and within the crown, respectively. As in the parsimony solution, the Bolca taxa †*Berybolcensis* and †*Tenuicentrum* are each other's closest relatives. This clade, along with †*Iridopristsis*, fall within an unresolved polytomy also including the lineage leading to the holocentrid crown.

We estimate divergence between polymixiids and our ingroup as 133.4 Mya (95% credible interval [CI]: 107.2–153 Mya) (Fig. 19). This split corresponds to the acanthomorph crown group in some phylogenomic analyses (Dornburg & Near, 2021). We estimate the divergence between Beryciformes and Trachichthyiformes (here represented by members of *Hoplostethus*) occurred at 110.7 Mya (95% CI: 91.4–132.3 Mya). Crown Beryciformes originated approximately 95.8 Mya (95% CI: 71.6–117.6 Mya). The last common ancestor of all holocentroids included in this analysis dates to 78.2 Mya (95% CI: 63–93.9 Mya), when †*Iridopristsis parrisi*, †*Berybolcensis* and †*Tenuicentrum* split from the lineage leading to Holocentridae. We estimate the age of the holocentrid crown as 61.3 Mya (95% CI: 50.6–75 Mya). The age of the last common ancestor of all myripristines included in the analysis is estimated as 40.9 Mya (95% CI: 32.7–50.7 Mya), with the crown Myripristinae dated to 34.8 Mya (95% CI: 26.7–43.5 Mya). The Ypresian taxon †*Eoholocentrum* splits from the crown members of Holocentrinae at 51.3 Mya (95% CI: 49.4–64 Mya), with the age of the holocentrine crown estimated as 33.8 Mya (95% CI: 26.7–42.1 Mya).

**Character-state mapping.** Mapping character states on the agreement subtree permits identification of possible synapomorphies of clades consistently recovered across our analyses. Several characters optimize to the clade comprising *Beryx* and Holocentroidea (Fig. 18B, a): expansion of the last pleural rib in the mediolateral plane (character 10, state 1); fusion of the second ural centrum to the combined first ural centrum and first preural centrum (character 11, state 1); loss of hypural six (character 12, state 1).

Holocentroidea, including †*Iridopristsis parrisi* (Fig. 18B, b), is supported by: the presence of a transverse crest of the supraoccipital (character 2, state 1); a separate opening for the orbital branch of the supraorbital sensory canal (character 3, state 1); a ventrolateral ‘winged’ expansion of the parasphenoid (character 6, state 1); an imperforate anterior ceratohyal (character 8, state 1); deep notches present along the ventral margin of the anterior ceratohyal (character 9, state 1); an expanded alveolar platform near the symphysis of the dentary that overhangs the lateral margin of the element (character 27, state 1); a concave premaxillary tooth gap at the mesial margin of the premaxilla, ventral to the ascending process (character 28, state 1).

The clade comprising Holocentroidea to the exclusion of †*Iridopristsis parrisi* (Fig. 18B, c) is supported by a dorsally projecting lamina anterior to the jaw joint of the anguloarticular (character 82, state 1).

Myripristinae (Fig. 18B, d) is supported by: a lateral connection of the otic bulla to the swim bladder (character 50, state 1); a prootic with an elongate process projecting laterally ventral to the pars jugularis foramen (character 51, state 1).

The clade comprising Holocentrinae, inclusive of †*Eoholocentrum* (Fig. 18B, e), is supported by: an edentulous ectopterygoid (character 30, state 1); 5 spinous procurrent caudal rays in the upper lobe and 4 in the lower lobe of the caudal fin (character 31, state 3); 16 preural caudal vertebrae (character 35, state 0).

The clade comprising Holocentrinae to the exclusion of †*Eoholocentrum* (Fig. 18B, f) is supported by: the ascending process of the premaxilla being as long as or longer than the alveolar process (character 19, state 1); the postmaxillary process of the premaxilla is anteroposteriorly short and dorsoventrally high (character 20, state 1); the first two circumorbitals with a depth to length ratio between 1:4.5 and 1:7 (character 21, state 1); the shaft of the maxilla is dorsoventrally deep and anteroposteriorly short (character 22, state 1); the loss of the expanded alveolar platform near the symphysis of the dentary (character 27, state 0); absence of the concave premaxillary tooth gap at the mesial margin of the premaxilla, ventral to the ascending process (character 28, state 0); the first dorsal fin pterygiophore inserts into a pocket on the

anterior margin of the neural spine of the second vertebra (character 76, state 1); the lachrymal has a wide-based, ventrally directed, and short spine (character 78, state 1); a single preopercular spine (character 79, state 1).

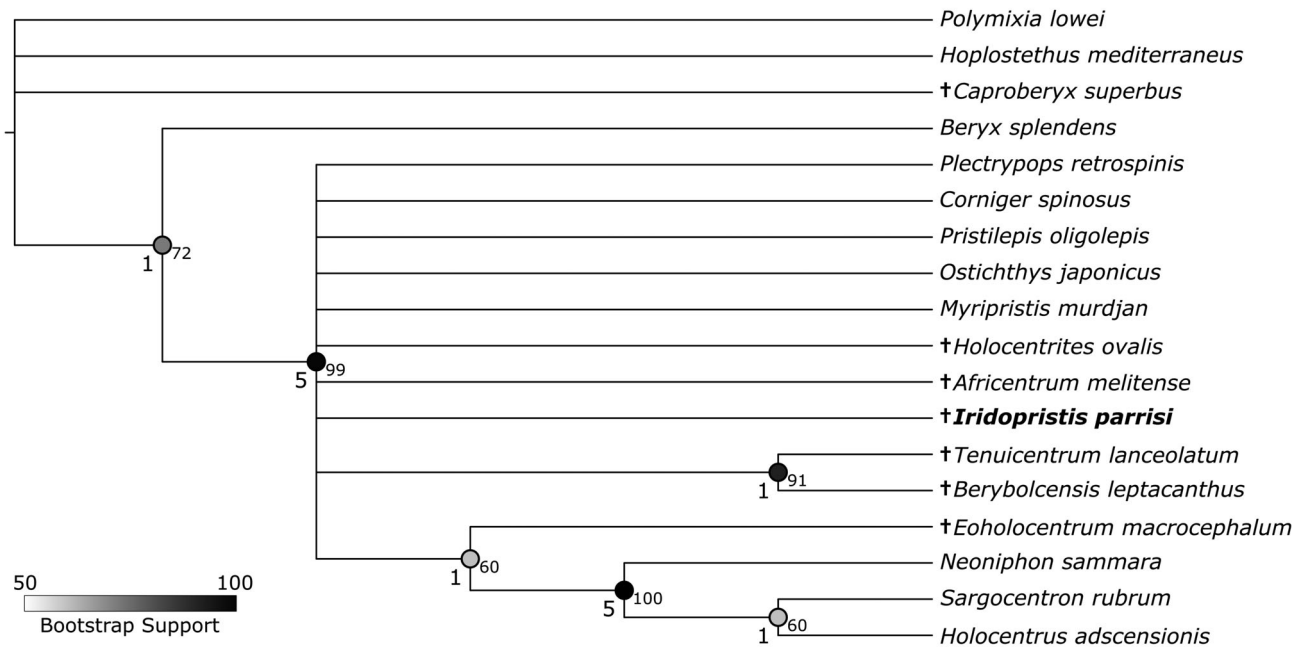
## Discussion

### Inferred relationships and implications for character evolution

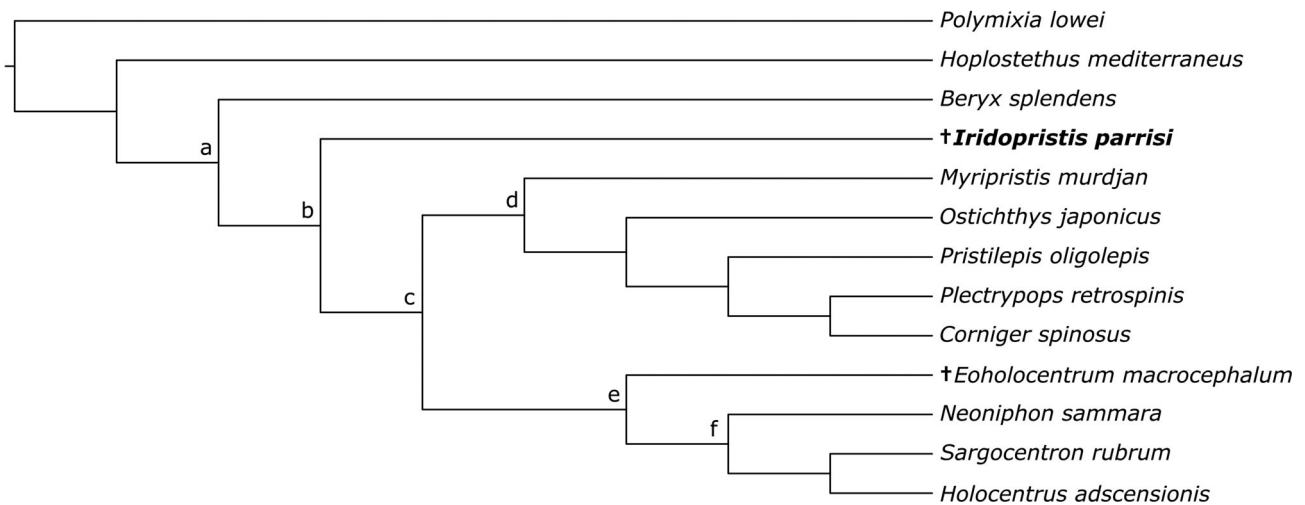
With respect to relationships among holocentroids, the results of both our parsimony and Bayesian analyses

show broad agreement with past solutions (e.g. Dornburg *et al.*, 2015), apart from our addition of †*Iridopristis*. The most notable exception is our placement of †*Africentrum* in a polytomy with the clades *Pristilepis* + *Ostichthys* and *Corniger* + *Plectrypops*, rather than as sister to *Myripristis* as previously reported (e.g. Dornburg *et al.*, 2015). Dornburg *et al.* (2015) did not indicate support for the hypothesized sister-group relationship between †*Africentrum* and *Myripristis*, although we note that our placement of †*Africentrum* is only weakly supported (posterior value of 62) and could easily change in subsequent analyses. Our placement of

A



B



†*Caproberyx* is also noteworthy. This Late Cretaceous taxon is generally regarded as an early holocentroid (Murray, 2016; Patterson, 1964), but we have found little evidence for this placement. Indeed, without constraining †*Caproberyx* to the ingroup it falls into a basal polytomy. Our constrained analysis places †*Caproberyx* as sister to Trachichthyiformes with weak posterior support (posterior value = 53) (Fig. 19). Past interpretations of †*Caproberyx* rely on verbal arguments enlisting a series of general traits: a shortened premaxillary process, lack of a preopercular spine (to align it with myripristines), rudimentary ridges of the frontals, teeth on the ectopterygoid (to align it with holocentrines), enlargement of the frontals in relation to all other neurocranial components, enclosure of the suborbital sensory canal on the lachrymal (to align it with holocentrids in general), as well as a ballooned ‘otic bulla’ (common in holocentrids, berycids, and trachichthyiforms) (Patterson, 1964; Regan, 1911). Many of these traits can be interpreted as plesiomorphic for acanthomorphs in general, rather than apomorphies that would suggest a closer affinity to holocentrids for †*Caproberyx*. Additionally, †*Caproberyx* lacks a spina occipitalis, a character present in †*Iridopristsis* and living holocentrids, berycids, and trachichthyids – but conspicuously absent from extant polymixiids and a number of other acanthomorph lineages (Davesne et al., 2016). Problems surrounding the placement of †*Caproberyx* likely apply to other Late Cretaceous acanthomorphs traditionally identified as ‘holocentroids’ (*sensu* Patterson, 1993), including †*Stichocentrus* (Patterson, 1967), †*Alloberyx* (Gaudant, 1969), †*Kansius* (Bardack, 1976) and †*Pelotius* (Gallo-Da-Silva & De Figueiredo, 1999). In contrast to the substantial progress that has been made

in placing early fossil representatives of other deeply diverging acanthomorph groups like percopsiforms (Murray et al., 2020) and lampriforms (Davesne et al., 2014; Delbarre et al., 2015), there is little clarity on the relationships of Cretaceous ‘beryciforms’ *sensu lato*. These taxa represent nearly 50% of Late Cretaceous acanthomorph generic richness (Murray, 2016), and persistent uncertainty surrounding their phylogenetic affinities represent an outstanding gap in our understanding of the early diversification of spiny-rayed fishes. An inclusive phylogenetic analysis of early fossil acanthomorphs – including fossil and modern representatives of the deepest branching lineages – should be a priority for future work. Apart from providing insight on the placement of specific fossil taxa, this approach might also help to clarify relationships among the earliest diverging extant acanthomorph lineages, which remain an area of conflict among recent phylogenetic hypotheses (Cantalice et al., 2021; Davesne et al., 2016).

Our analyses provide a new perspective on previous verbal assessments of the possibly phylogenetic affinities of the materials formally described here as †*Iridopristsis parrisi*. In his review of Cretaceous acanthomorphs from North America, Stewart (1996) mentioned these specimens (specifically referring to NJSM GP12145), which he considered Maastrichtian in age. His general assessment of their affinities anticipates our hypothesis, with the New Jersey fossils in some ways “intermediate between other Cretaceous holocentrids and the two Cenozoic subfamilies of Holocentridae” (Stewart, 1996, p. 392). He also noted that this form shared a potential synapomorphy with myripristines (not explicitly mentioned, but we assume it was the expanded symphyseal margin of the dentary and the

←

**Figure 18.** Holocentroid relationships inferred from a maximum parsimony analysis of morphological data. **A**, strict consensus of 588 most parsimonious trees with tree length = 112 steps. Circles at nodes indicate bootstrap support values between 50 (white) and 100 (black). Bremer support indices indicated by numbers adjacent to nodes. †*Iridopristsis parrisi* in bold. **B**, agreement subtree of 588 most-parsimonious trees with length = 112 steps. Letters at nodes indicate character states supporting clades of interest. Character states for characters 1–80 described in detail in Dornburg et al. (2015). Characters 81 and 82 new to this paper. Character-state optimizations keyed to characters at nodes: (a) 10[1], last pleural rib expanded in mediolateral plane; 11[1], second ural centrum fused to the combined first ural centrum and first preural centrum; 12[1], loss of hypural six. (b) 2[1], transverse crest of the supraoccipital; 3[1], separate opening of the orbital branch of the supraorbital sensory canal; 6[1], ventrolateral wings of the parasphenoid; 8[1], anterior ceratohyal with no foramen (closed ontogenetically); 9[1], deep notches on the ventral margin of the anterior ceratohyal to accommodate branchiostegals; 27[1], alveolar platform expanded near the symphysis to overhang the lateral margin of the dentary; 28[1], concave premaxillary tooth gap at the mesial margin. (c) 82[1], dorsally projecting lamina anterior to the jaw joint on the anguloarticular. (d) 50[1], lateral connection of the otic bulla to the swim bladder; 51[1], prootic with an elongate process projecting laterally ventral to the pars jugularis foramen. (e) 30[0], loss of teeth on the ectopterygoid; 31[3], five spinous procurrent caudal rays in upper lobe and four in lower lobe; 35[0] 16 preural caudal vertebrae. (f) 19[1], ascending process of the premaxilla as long as or longer than the alveolar process; 20[1], postmaxillary process of the premaxilla anteroposteriorly short and dorsoventrally high; 21[1], depth to length ratio of first two circumorbitals between 1:4.5 and 1:7; 22[1], shaft of the maxilla dorsoventrally deep and anteroposteriorly short; 27[0], loss of alveolar platform expansion near the symphysis to overhang the lateral margin of the dentary; 28[0], loss of convex premaxillary tooth gap at the mesial margin; 76[1], first dorsal fin pterygiophore inserts into a pocket on the anterior margin of the neural spine of the second vertebra; 78[1], lachrymal with a wide-based, ventrally directed, and short spine; 79[1], single preopercular spine in adults.

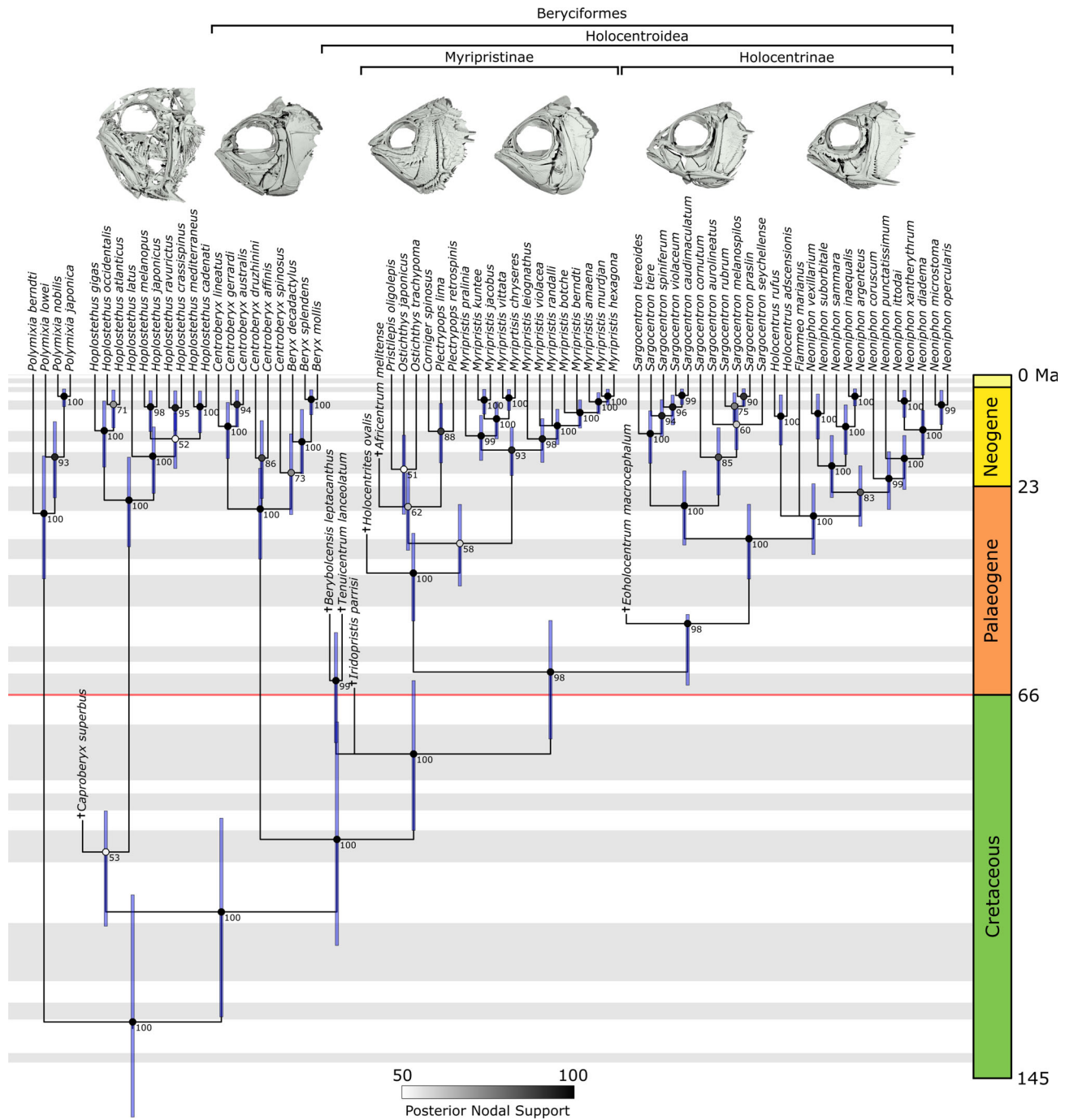


**Figure 19.** Maximum clade credibility tree for a total-evidence analysis of holocentroid interrelationships. Bars at nodes represent 95% HPD (highest posterior density) for node age. Nodal supported indicated as posterior probabilities between 50 (white) and 100 (black). The Cretaceous–Palaeogene boundary is highlighted in red.

edentulous tooth gap along the mesial margin of the pre-maxilla based on features visible externally), but also indicated some uncertainty about potential homoplasy in this or other characters. Stewart (1996) also stated that these specimens likely belonged to †*Beryx insculptus*, which he regarded as incorrectly attributed to Berycidae.

That species is based on a poorly preserved patch of scales from the Maastrichtian Navesink Formation and lacks obvious diagnostic characters (Supplemental Material Figure 1C), and we do not consider †*Iridopristsis parrisi* referable to it. Using  $\mu$ CT to non-destructively sample the otolith morphology,

Schwarzhan et al. (2018) provided additional information bearing on the Hornerstown holocentroid specimens. They interpreted NJSM GP12145 and GP12381 as belonging to the holocentrine subclade, based on the generalized otolith morphology in comparison to myripristines (Fig. 16).

As anticipated by Stewart (1996), the identification of †*Iridopristsis* as a stem holocentrid has important implications for patterns of character evolution in squirrelfishes and soldierfishes. †*Iridopristsis* bears a mosaic of characters that, while consistent with its placement on the holocentrid stem, call into question the status of previously proposed synapomorphies of extant holocentrid lineages. Most significant are the expansion of the alveolar platform of the dentary and the premaxillary tooth gap. Both traits are present in †*Iridopristsis*, but have been interpreted as myripristine synapomorphies (Dornburg et al., 2015; Marramà et al., 2021; Stewart, 1984). Instead, our results suggest that these are more general features, probably present in the last common ancestor of Cenozoic holocentroids. Future work should seek additional morphological evidence for myripristine monophyly, which is strongly supported by molecular data. By contrast, character evidence for holocentrine monophyly (e.g. including an ascending process of the premaxilla as long as or longer than the alveolar process) is unaffected by the combination of characters apparent in †*Iridopristsis*.

†*Iridopristsis parrisi* bears two noteworthy features undescribed in other holocentroids and not seen in fossil relatives: (1) a flat, unexpanded auditory ‘bulla’, and (2) an unornamented triangular facet on the posterolateral surface of the maxilla. All extant and three-dimensionally preserved fossil berycimorph fishes, with the exception of †*Iridopristsis parrisi*, bear varying degrees of ‘ballooning’ on the lateral surface of the otic chamber (Patterson, 1964). However, ‘ballooning’ of the otic chamber is difficult to assess in somewhat flattened material of †*Tenuicentrum*, †*Berybolcensis*, and †*Eoholocentrum* from Bolca. In the case of the facet on the posterolateral surface of the maxilla, it is notable that specimens of *Myripristis murdjan* and *Ostichthys japonicus* possess a thin lamina tightly associated with the maxilla at this same position. In the case of *M. murdjan*, this lamina is only apparent in tomographical sections. †*Ctenothrissa radians* (Agassiz, 1835) bears a maxillary facet (Patterson, 1964, p. 232; Fig. 9) remarkably similar to the one found on the maxilla of †*Iridopristsis* (Fig. 8). Patterson refers to this facet as a groove for the insertion of ligaments associated with the adductor muscles of the mandible, while Smith Woodward (1903) suggests that this groove may be a sensory canal. Neither of these explanations seem likely,

given the thin lamination seen in this location in the aforementioned extant holocentrids.

### Evolutionary timescale

Our estimated timescales broadly match those presented in earlier analyses, with substantial overlap between HPD intervals for nodes shared between studies. Challenges in comparing age estimates for the oldest nodes in our tree reflect contrasting taxon samples and fundamental disagreements about branching patterns deep within acanthomorph phylogeny. Most recent phylogenetic solutions (Alfaro et al., 2018; Dornburg & Near, 2021; Hughes et al., 2018) agree that the root node in our analysis, indicating the divergence between polymixiids and the clade comprising trachichthyids, berycids and holocentroids, represents the acanthomorph crown node. We estimate this divergence as 133.4 Mya (95% CI: 107.2–153 Mya), which is somewhat younger than was found by previous authors (Rabosky et al., 2018: 137.9 Mya (no 95% CI: inferred under likelihood); Alfaro et al., 2019: 139.6 Mya (95% CI: 130.8–147 Mya); Hughes et al., 2019: 144 Mya (95% CI: 136.8–152 Mya)). Our analysis, which finds Trachichthyiformes as sister to Beryciformes + Holocentroidea, matches the topology presented by Rabosky et al. (2018), although our analysis does not sample percomorphs. Our inferred divergence time of 110.7 Mya (95% CI: 91.4–132.3 Mya) between Trachichthyiformes and Beryciformes inclusive of Holocentroidea is younger than was found by Rabosky et al. (2018: 124.8 Mya (no 95% CI: inferred under likelihood)), although that previous age value falls within the uncertainty for our estimates. Hughes et al. (2018) recovered a different pattern of relationships among these groups, finding that a clade comprising Trachichthyiformes + Beryciformes represents the sister lineage of Holocentroidea + Percomorpha. Their estimated divergence of 131.9 Mya (95% CI: 126.2–137.6 Mya) between holocentroids and trachichthyiforms is also older than our estimate for the equivalent node (Hughes et al., 2019). Likewise, Alfaro et al. (2019) recovered a topology with Trachichthyiformes as sister to a clade comprising Beryciformes + Holocentroidea sister to Percomorpha, and recovered a divergence estimate of 133.5 Mya (95% CI: 121.9–144.3 Mya) for the equivalent node.

Our estimate for the age of crown-group Holocentridae (subclades Myripristinae + Holocentrinae) of 61.3 Mya (95% CI: 50.6–75.1 Mya) is in close agreement with ages inferred by node-calibrated (Rabosky et al., 2018: 56 Mya [no 95% CI: inferred under likelihood]; Hughes et al., 2019: 54 Mya [95% CI: 50.2–57.9 Mya]; Alfaro et al., 2018: 61.5 Mya [95% CI: 49–77.6

Mya]) and tip-dated (Dornburg *et al.*, 2015: 54.7 Mya) topologies. These studies support an origin of crown holocentrids postdating the K/Pg extinction. This inference is broadly consistent with the affinities of most early Cenozoic holocentroid body fossils, the majority of which represent stem holocentrids. However, uncertainty surrounding the timing of the split between myripristines and holocentrines means that an earlier divergence cannot be rejected.

Of existing studies, only Dornburg *et al.* (2015) samples holocentrids densely enough to permit detailed comparison of estimated divergence times within the clade. Our results agree with most of the node-age estimates presented by Dornburg *et al.* (2015), with one conspicuous difference: the divergence between †*Africentrum* and its closest living relatives. Dornburg *et al.* (2015) found †*Africentrum* to be the sister lineage of *Myripristis*, with the divergence of these lineages estimated at 15 Mya. We inferred a slightly different position for †*Africentrum* as sister to the myripristine subclade including the genera *Pristilepis*, *Ostichthys*, *Corniger* and *Plectrypops*. Our analysis estimates this divergence at 27.2 Mya (95% CI: 20.2–36.2 Mya). This deeper divergence reflects a revised tip age for †*Africentrum*. Dornburg *et al.* (2015) applied an age of ~10 Mya for †*Africentrum*, while we use the earliest age for the genus (calibrated as a uniform distribution ranging from 17.154 to 17.466 Mya) based on available geological evidence.

Our evolutionary timescale is also broadly consistent with the distribution of holocentroid otoliths, which offer a semi-independent palaeontological timescale to that of the body fossils explicitly incorporated into our analyses. The oldest fossil otoliths attributed to the subfamily Myripristinae derive from the Ypresian-age London Clay Formation (Nolf, 2013), suggesting that myripristines acquired their distinctive otolith morphology (character 81, state 1; Fig. 16C) during, or prior to, this time interval. Meanwhile, the oldest fossil otoliths attributed to Holocentrinae derive from the Maastrichtian-age Gerhartsreiter Beds (Nolf, 2013; Schwarzhans, 2010). †*Iridopristsis parrisi* possesses an otolith morphology that, in isolation, is consistent with the primitive arrangement retained by Holocentrinae (character 81, state 0; Fig. 16A, D) (Schwarzhans *et al.*, 2018), while its morphology taken as a whole suggests that it is a stem-member of Holocentridae (Fig. 18). This raises the possibility that Maastrichtian otoliths attributed to Holocentrinae (i.e. †*Sillaginocentrus aliena* [Schwarzhans, 2010], †*Traubiella anagoformis* [Schwarzhans, 2010], †*Holocentronotus percomorpha* [Schwarzhans, 2010], and †*Pfeilichthys pfeili* [Schwarzhans, 2010] [Nolf, 2013; Schwarzhans, 2010])

could, like †*Iridopristsis*, be stem rather than crown holocentrids.

### Patterns of evolutionary diversification and geographical distribution in holocentroids

Our phylogenetic interpretation of †*Iridopristsis parrisi* has possible implications for two key aspects of marine fish evolution in the early Cenozoic: responses to the K/Pg extinction (Alfaro *et al.*, 2018; Sibert & Norris, 2015) and shifting geographical patterns of marine biodiversity (Cowman *et al.*, 2017; Dornburg *et al.*, 2015). The majority-rule fossilized birth–death topology implies that several holocentrid lineages survived the K/Pg boundary (Fig. 19), and indicates that the divergence of Myripristinae and Holocentrinae probably – but not certainly – occurred in the early Palaeogene. This result agrees with previous studies where the Myripristinae and Holocentrinae were resolved as originating in the wake of the K/Pg extinction event (Alfaro *et al.*, 2018; Dornburg *et al.*, 2015; Hughes *et al.*, 2018; Rabosky *et al.*, 2018). The holocentrid lineages represent an important component of modern reef fish faunas, the expansion of which in the Paleocene have been interpreted as being the result of the geographical expansion of scleractinian corals during this interval (Bellwood *et al.*, 2017; Price *et al.*, 2014).

†*Iridopristsis* also bears on debates concerning Cenozoic marine fish biogeography. Most Cenozoic holocentroid body fossils come from a region around the contemporary Mediterranean, representing the ancient West Tethys. This has led some to hypothesize that modern squirrelfishes evolved in this region (Dornburg *et al.*, 2015; Marramà *et al.*, 2021), an interpretation consistent with a major biogeographical hypothesis placing the West Tethys as the nexus of marine biodiversity in the early Cenozoic prior to the establishment of the contemporary hotspot in the Indo-Pacific by the Miocene (Renema *et al.*, 2008). This scenario enjoys support from the fossil record of invertebrates (Bellwood *et al.* 2012; Renema *et al.*, 2008; Saulsbury & Baumiller, 2022), as well as from studies that integrate palaeontological evidence with molecular phylogenies (Cowman *et al.*, 2017; Dornburg *et al.*, 2015; Siqueira *et al.*, 2019). The geographical patchiness of the fossil record represents a serious obstacle to evaluating these hypotheses for fishes. This is amplified by the stratigraphical and geographical alignment of the remarkable Bolca fauna with the early Palaeogene West Tethyan hotspot (Friedman & Carnevale, 2018). While this exceptional fossil snapshot provides a significant window into this region during a critical time in the past, it also dominates our understanding of the early history of holocentroids and other marine fish groups

(Dornburg et al., 2015). This problem extends beyond Bolca, with the European record providing most of the significant early Cenozoic marine fish faunas represented by body fossils (Friedman & Carnevale, 2018; Friedman et al., 2016). As a consequence, there are comparatively few fossils of early Palaeogene age from outside the Tethys that can be placed in phylogenetic trees, raising questions about the relative influence of biological pattern and sampling bias on biogeographical hypotheses for marine fishes incorporating palaeontological data. Fossils provide unique data that can overturn inferences of ancestral states, ecologies, and geographical ranges based on living taxa alone (Betancur-R. et al., 2015; Finarelli & Flynn, 2006; Wisniewski et al., 2022). However, the inclusion of fossil data might cause misleading inferences of past ranges if there are substantial spatial heterogeneities in sampling or major geographical gaps in the record. Recent biogeographical work on marine invertebrates has applied taphonomical analogues to help determine whether the absence of fossils from particular regions might be meaningful (Saulsbury & Baumiller, 2022), but this approach has not been applied to fishes. Detailed accounts of fossils from regions not well represented in the literature represent an important step in building a more complete picture of biogeographical patterns in these groups. By virtue of its geographical provenance alone, †*Iridopristsis* suggests a more complicated distributional history for early Palaeogene holocentroids than past analyses (Dornburg et al., 2015). However, it is premature to speculate more on aspects of holocentrid biogeographical history without a better understanding of the composition of deeper parts of the stem and the Palaeogene marine fish fossil record outside the Tethys more generally.

## Conclusions

†*Iridopristsis parrisi* presents as an articulated skull and abdomen from the early Danian Hornerstown Formation of New Jersey, USA. Inclusion of the specimen in a phylogenetic analysis suggests that it is a stem-member of Holocentridae, along with the Ypresian-age †*Berybolcensis* and †*Tenuicentrum*. The new species possesses multiple characters that align it more closely to Cenozoic holocentroids than to Cretaceous holocentroids, including: a separate opening of the orbital branch of the supraorbital sensory canal, ventrolateral wings of the parasphenoid, an anterior ceratohyal with no foramen, and deep notches along the ventral margin of the anterior ceratohyal to accommodate branchiostegals. Character state optimization supports character state acquisitions prior to the origin of

†*Iridopristsis parrisi* that have previously been interpreted as derived states for the subclade Myripristinae: an alveolar platform expanded near the symphysis to overhang the lateral margin of the dentary, and a concave tooth gap at the mesial margin of the premaxilla. This finding necessitates a deeper examination of phenotypic synapomorphies to support the subfamily Myripristinae. Three-dimensionally preserved fossil fishes of Danian age are rare, and further excavation of the greensand formations along the mid-Atlantic of the USA may offer greater insight into the faunal composition and evolutionary dynamics during the critical early Palaeogene history of marine spiny-rayed fishes.

## Acknowledgements

We thank two anonymous reviewers for their helpful feedback, as well as the editorial board of the Journal of Systematic Palaeontology for their patience and assistance in formatting this manuscript. We thank D. C. Parris, D. Ehret and R. Pellegrini (NJSM GP) for access to the material herein described. We thank W. Simpson and L. Grande (FMNH) for access to comparative fossil materials, and D. Nelson and R. Singer (UMMZ), M.H. Sabaj and M. Arce-H. (ANSP), and S. Mochel and C. McMahan (FMNH) for access to extant comparative materials. Collections support from A. Rountrey, B. Dergis and L. Sandefur (UMMP) was necessary for the completion of this project. D. Goodvin greatly assisted with the  $\mu$ CT segmentation process. Discussions with G. Carnevale, D. C. Parris and A. Capobianco aided in phylogenetic reconstruction and constraining ages of taxa included in the analysis. Generation of renders was greatly aided by the instruction of A. Capobianco and R. T.-Figueroa. This study includes data produced in the CTEES facility at University of Michigan, supported by the Department of Earth & Environmental Sciences and College of Literature, Science, and the Arts. This work was supported in part by the University of Michigan Department of Earth and Environmental Sciences (Scott Turner Award to J.V.A.), University of Michigan Rackham Graduate School (Rackham Merit Fellowship to J.V.A.), the Society of Systematic Biologists (Graduate Student Research Award to J.V.A.), and the Paleontological Society (Harry B. Wittington Award to J.V.A.).

## Supplemental material

Data associated with this study are available on Figshare ([10.6084/m9.figshare.21754541](https://doi.org/10.6084/m9.figshare.21754541)). Supplemental



material for this article can be accessed here: <https://doi.org/10.1080/14772019.2023.2168571>

## ORCID

James V. Andrews  <http://orcid.org/0000-0001-7093-1335>

Matt Friedman  <http://orcid.org/0000-0002-0114-7384>

## References

- Agassiz, L. (1833–1844). *Recherches sur les poisons fossils*. 5 vols. Imprimerie de Petitpierre.
- Alfaro, M. E., Faircloth, B. C., Harrington, R. C., Sorenson, L., Friedman, M., Thacker, C. E., Oliveros, C. H., Cerný, D., & Near, T. J. (2018). Explosive diversification of marine fishes at the Cretaceous–Paleogene boundary. *Nature Ecology & Evolution*, 2, 688–696. <https://doi.org/10.1038/s41559-018-0494-6>
- Alfaro, M. E., Faircloth, B. C., Harrington, R. C., Sorenson, L., Friedman, M., Thacker, C. E., Oliveros, C. H., Cerný, D., & Near, T. J. (2019). Explosive diversification of marine fishes at the Cretaceous–Paleogene boundary [Data set]. *Dryad*. <https://doi.org/10.5061/dryad.085dd>
- Alvarado-Ortega, J., Cuevas-García, M., Melgarejo-Damián, M. P., Cantalice, K. M., Alaniz-Galvan, A., Solano-Templos, G., & Than-Marchese, B. A. (2015). Paleocene fishes from Palenque, Chiapas, southeastern Mexico. *Palaeontologia Electronica*, 18, 1–22. <https://doi.org/10.26879/536>
- Alvarado-Ortega, J., & Than-Marchese, B. A. (2013). The first record of a North American Cenomanian Trachichthyidae fish (Acanthomorpha, Acanthopterygii), *Pepemkay maya*, gen. et sp. nov., from El Chango Quarry (Sierra Madre Formation), Chiapas, Mexico. *Journal of Vertebrate Paleontology*, 33, 48–57. <https://doi.org/10.1080/02724634.2012.712585>
- Alvarez, L. W., Alvarez, W., Asaro, F., & Michel, H. V. (1980). Extraterrestrial cause for the Cretaceous–Tertiary extinction. *Science*, 208, 1095–1108. <https://doi.org/10.1126/science.208.4448.1095>
- Argyriou, T., & Davesne, D. (2021). Offshore marine actinopterygian assemblages from the Maastrichtian–Paleogene of the Pindos Unit in Eurytania, Greece. *Paleontology and Evolutionary Science, PeerJ*, 9, e10676. <https://doi.org/10.7717/peerj.10676>
- Bardack, D. (1976). Paracanthopterygian and acanthopterygian fishes from the Upper Cretaceous of Kansas. *Fieldiana, Geology*, 33, 355–374.
- Bassani, F. (1876). Pesci fossili nuovi del calcare eoceno di Monte Bolca. *Atti della Società Veneto-Trentina di Scienze Naturali residente in Padova*, 5, 151.
- Bassani, F. (1911). Sopra un Bericidae del calcare miocenico di Lecce, di Rosignano piemonte e di Malta. *Atti della Reale Accademia della Società Fische e Matematiche di Napoli*, 15, 1–13.
- Becker, M. A., Chamberlain, J. A., Lundberg, J. G., L'Amoreaux, W. J., Chamberlain, R. B., & Holden, T. M. (2009). Beryciform-like fish fossils (Teleostei: Acanthomorpha: Euacanthopterygii) from the Late Cretaceous–Early Tertiary of New Jersey. *Proceedings of the Academy of Natural Sciences of Philadelphia*, 158, 159–181. <https://doi.org/10.1635/053.158.0108>
- Bellwood, D. R., Renema, W., & Rosen, B. R. (2012). Biodiversity hotspots, evolution and coral reef biogeography: a review. In D. J. Gower, K. G. Johnson, J. E. Richardson, B. R. Rosen, L. Rüber & S. T. Williams (Eds.), *Biotic Evolution and Environmental Change in Southeast Asia* (pp. 216–245). Cambridge University Press.
- Bellwood, D. R., Goatley, C. H., & Bellwood, O. (2017). The evolution of fishes and corals on reefs: form, function and interdependence. *Biological Reviews*, 92, 878–901. <https://doi.org/10.1111/brv.12259>
- Betancur-R., R., Ortí, G., & Pyron, R. A. (2015). Fossil-based comparative analyses reveal ancient marine ancestry erased by extinction in ray-finned fishes. *Ecology Letters*, 18, 441–450. <https://doi.org/10.1111/ele.12423>
- Betancur-R., R., Wiley, E. O., Arratia, G., Acero, A., Bailly, N., Miya, M., Lecointre, G., & Ortí, G. (2017). Phylogenetic classification of bony fishes. *BMC Evolution and Evolution*, 17, 162. <https://doi.org/10.1186/s12862-017-0958-3>
- Blainville, H. D. de. (1818). *Poissons fossiles. Nouveau dictionnaire d'histoire naturelle, appliquée aux arts, à l'agriculture, à l'économie rurale et domestique, à la médecine, etc.* (Vol. 27, pp. 349). Chez Deterville, 1816–1819.
- Boles, Z. M. (2016). *Vertebrate taphonomy and paleoecology of a Cretaceous–Paleogene marine bonebed*. Unpublished PhD thesis, Drexel University, 263 pp.
- Cantalice, K. M., Than-Marchese, B. A., & Villalobos-Segura, E. (2021). A new Cenomanian acanthomorph fish from the El Chango quarry (Chiapas, south-eastern Mexico) and its implications for the early diversification and evolutionary trends of acanthopterygians. *Papers in Palaeontology*, 7, 1699–1726. <https://doi.org/10.1002/spp2.1359>
- Carranza-Becerra, B. (2020). *Determinación taxonómica de un pez fósil del orden Holocentriformes (Teleostei, Acanthopterygii) del Cretácico Superior de Chiapas, México* [Unpublished Bachelors Thesis]. Universidad Nacional Autónoma de México.
- Casier, E., & Stinton, F. C. (1966). *Faune ichthyologique du London Clay. Trustees of the British Museum (Natural History)*.
- Chang, J., Rabosky, D. L., Smith, S. A., & Alfaro, M. E. (2019). An R package and online resource for macroevolutionary studies using the ray-finned fish tree of life. *Methods in Ecology and Evolution*, 10, 1118–1124. <https://doi.org/10.1111/2041-210X.13182>
- Conrad, G. M. (1941). A fossil squirrel-fish from the Upper Eocene of Florida. Contributions to Florida Vertebrate Paleontology. *Geological Bulletin*, 22, 9–25.
- Cope, E. D. (1869). Second addition to the history of fishes of the Cretaceous of the United States. *Proceedings of the American Philosophical Society*, 11, 240–244.
- Cowman, P. F., Parravicini, V., Kulbicki, M., & Floeter, S. R. (2017). The biogeography of tropical reef fishes: endemism and provinciality through time. *Biological Reviews*, 92, 2112–2130. <https://doi.org/10.1111/brv.12323>

- Cuvier, G.** (1829). *Le règne animal distribué d'après son organisation, pour servir de base à l'histoire naturelle des animaux et d'introduction à l'anatomie comparée, Vol. 2.* Chez Déterville.
- Dalton, R. F., Monteverde, D. H., Sugarman, P. J., & Volkert, R. A.** (2014). *Bedrock Geological Map of New Jersey. Scale 1 to 250,000.* New Jersey Geological and Water Survey.
- Datovo, A., & Vari, R. P.** (2013). The jaw adductor muscle complex in Teleostean fishes: Evolution, homologies and revised nomenclature (Osteichthyes: Actinopterygii). *PLoS ONE*, 8, e60846. <https://doi.org/10.1371/journal.pone.0060846>
- Davesne, D., Friedman, M., Barriel, V., Lecointre, G., Janvier, P., Gallut, C., & Otero, O.** (2014). Early fossils illuminate character evolution and interrelationships of Lampridiformes (Teleostei, Acanthomorpha). *Zoological Journal of the Linnean Society*, 172, 475–498. <https://doi.org/10.1111/zoj.12166>
- Davesne, D., Gallut, C., Barriel, V., Janvier, P., Lecointre, G., & Otero, O.** (2016). The phylogenetic intrarelationships of spiny-rayed fishes (Acanthomorpha, Teleostei, Actinopterygii): Fossil taxa increase the congruence of morphology with molecular data. *Frontiers in Ecology and Evolution*, 4, 129. <https://doi.org/10.3389/fevo.2016.00129>
- Delbarre, D. J., Davesne, D., & Friedman, M.** (2015). Anatomy and relationships of †*Aipichthys pretiosus* and †*Aipichthys nuchalis* (Acanthomorpha: Lampridomorpha), with a review of Late Cretaceous relatives of oarfishes and their allies. *Journal of Systematic Palaeontology*, 14, 545–567. <https://doi.org/10.1080/14772019.2015.1078538>
- Dixon, F.** (1850). *The geology and fossils of the Tertiary and Cretaceous formations of Sussex.* Longman, Brown, Green and Longmans.
- Dornburg, A., Moore, J., Beaulieu, J. M., Eytan, R. I., & Near, T. J.** (2015). The impact of shifts in marine biodiversity hotspots on patterns of range evolution: Evidence from the Holocentridae (squirrelfishes and soldierfishes). *Evolution*, 69, 146–161. <https://doi.org/10.1111/evo.12562>
- Dornburg, A., Moore, J. A., Webster, R., Warren, D. L., Brandley, M. C., Iglesias, T. L., Wainwright, P. C., & Near, T. J.** (2012). Molecular phylogenetics of squirrelfishes and soldierfishes (Teleostei: Beryciformes: Holocentridae): Reconciling more than 100 years of taxonomic confusion. *Molecular Phylogenetics and Evolution*, 65, 727–738. <https://doi.org/10.1016/j.ympev.2012.07.020>
- Dornburg, A., & Near, T. J.** (2021). The emerging phylogenetic perspective on the evolution of actinopterygian fishes. *Annual Review of Ecology, Evolution, and Systematics*, 52, 427–452. <https://doi.org/10.1146/annurev-ecolsys-122120-122554>
- Dornburg, A., Townsend, J. P., Brooks, W., Spriggs, E., Eytan, R. I., Moore, J. A., Wainwright, P. C., Lemmon, A., Lemmon, E. M., & Near, T. J.** (2017). New insights on the sister lineage of percomorph fishes with an anchored hybrid enrichment dataset. *Molecular Phylogenetics and Evolution*, 110, 27–38. <https://doi.org/10.1016/j.ympev.2017.02.017>
- Dunkle, D. H., & Olsen, S. J.** (1959). Description of a beryciform fish from the Oligocene of Florida (Florida Geological Survey Special Publication 2 (3)), Tallahassee. <https://doi.org/10.35256/SP02P3>
- Esmeray-Senlet, S., Miller, K. G., Sherrell, R. M., Senlet, T., Vellekoop, J., & Brinkhuis, H.** (2017). Iridium profiles and delivery across the Cretaceous/Paleogene boundary. *Earth and Planetary Science Letters*, 457, 117–126. <https://doi.org/10.1016/j.epsl.2016.10.010>
- Finarelli, J. A., & Flynn, J.** (2006). Ancestral state reconstruction of body size in the Caniformia (Carnivora, Mammalia): The effects of incorporating data from the fossil record. *Systematic Biology*, 55, 301–313. <https://doi.org/10.1080/10635150500541698>
- Forsskål, P.** (1775). *Descriptiones animalium, avium, amphibiorum, piscium, insectorum, vermium; quae in itinere orientali observavit Petrus Forsskål. Post mortem auctoris edidit Carsten Niebuhr.* Havenai, Mölleri.
- Friedman, M.** (2010). Explosive morphological diversification of spiny-finned teleost fishes in the aftermath of the end-Cretaceous extinction. *Proceedings of the Royal Society B*, 277, 1675–1683. <https://doi.org/10.1098/rspb.2009.2177>
- Friedman, M., Beckett, H. T., Close, R. A., & Johanson, Z.** (2016). The English Chalk and London Clay: two remarkable British bony fish Lagerstätten. In Z. Johanson, P. M. Barrett, M. Richter & M. Smith (Eds.), *Arthur Smith Woodward: His Life and Influence on Modern Vertebrate Palaeontology* (pp. 165–200). Geological Society. <https://doi.org/10.1144/SP430.18>
- Friedman, M., & Carnevale, G.** (2018). The Bolca Lagerstätten: shallow marine life in the Eocene. *Journal of the Geological Society*, 175, 569–579. <https://doi.org/10.1144/jgs2017-164>
- Gallagher, W. B.** (1995). Paleontology and stratigraphy of the Inversand Pit, Gloucester County, New Jersey. *Geological Association of New Jersey*, 12, 323–335.
- Gallagher, W. B.** (2002). Faunal changes across the Cretaceous–Tertiary (K–T) boundary in the Atlantic coastal plain of New Jersey: Restructuring the marine community after the K–T mass-extinction event. In C. Koeberl & K. G. MacLeod (Eds.) *Catastrophic Events and Mass Extinctions: Impacts and Beyond* (pp. 291–301). Geological Society of America Special Paper 356. <https://doi.org/10.1130/0-8137-2356-6.291>
- Gallagher, W. B., Miller, K. G., Sherrell, R. M., Browning, J. V., Field, M. P., Olsson, R. K., Sugarman, P. J., Tuorto, S., & Wahyudi, H.** (2012). On the last mosasaurs: Late Maastrichtian mosasaurs and the Cretaceous–Paleogene boundary in New Jersey. *Bulletin de la Société Géologique de France*, 183, 145–150. <https://doi.org/10.2113/gssgfbull.183.2.145>
- Gallagher, W. B., & Parris, D. C.** (1996). *Age determinations for Late Cretaceous dinosaur sites in the New Jersey coastal plain.* Sixth North American Paleontological Convention, Paleontological Society Special Publication Number 8.
- Gallo-Da-Silva, V., & De Figueiredo, F. J.** (1999). *Pelotius hessellae*, gen. et sp. nov. (Teleostei: Holocentridae) from the Cretaceous (Turonian) of Pelotas Basin, Brazil. *Journal of Vertebrate Paleontology*, 19, 263–270. <https://doi.org/10.1080/02724634.1999.10011140>
- Gaudant, M.** (1969). Sur quelques nouveaux poissons bérycoïdes crétacés du Mont Liban. *Notes et Mémoires sur le Moyen-Orient, Muséum National d'Histoire Naturelle*, 10, 273–283.

- Gayet, M.** (1980a). Recherches sur l'ichthyofaune céno manienne des Monts de Judée: les "acanthoptérygiens". *Annales de Paléontologie (Vertébrés)*, 66, 75–128.
- Gayet, M.** (1980b). Contribution à l'étude anatomique et systématique des poissons céno maniens du Liban, anciennement placés dans les acanthoptérygiens. *Mémoires du Muséum national d'histoire naturelle Série C Géologie*, 44, 1–149.
- Gilbert, C. H.** (1905). The deep-sea fishes of the Hawaiian Islands. In D. S. Jordan & B. W. Evermann (Eds.), *The aquatic resources of the Hawaiian Islands* (pp. 575–713). Bulletin of the United States Fish Commission, 23.
- Gilbert, C. H.** (1915). Fishes collected by the United States Fisheries steamer 'Albatross' in Southern California in 1904. *Proceedings of the U.S. National History Museum*, 48, 305–380.
- Grande, L., & Bemis, W. E.** (1998). A comprehensive phylogenetic study of amiid fishes (Amiidae) based on comparative skeletal anatomy. An empirical search for interconnected patterns of natural history. *Journal of Vertebrate Paleontology*, 18(Suppl. 1), 1–696. <https://doi.org/10.1080/02724634.1998.10011114>
- Guichenot, A.** (1853). Poissons. In R. de la Sagra (Ed.), *Histoire physique, politique et naturelle de l'île de Cuba* (Vol. 2, pp. 1–206). Arthur Bertrand.
- Guindon, S., Dufayard, J. F., Lefort, V., Anisimova, M., Hordijk, W., & Gascuel, O.** (2010). New algorithms and methods to estimate maximum-likelihood phylogenies: assessing the performance of PhyML 3.0. *Systematic Biology*, 59, 307–321. <https://doi.org/10.1093/sysbio/syq010>
- Günther, A.** (1859). *Catalogue of the acanthopterygian fishes in the collection of the British Museum. Gasterosteidae, Berycidae, Percidae, Aphredoderidae, Pristipomatidae, Mullidae, Sparidae*. Vol. 1. British Museum.
- Günther, A.** (1887). Report on the deep-sea fishes collected by H.M.S. 'Challenger' during the years 1873–1876. Report on the Scientific Results of the Voyage of H.M.S. Challenger. Vol. 22, Pt. 57. (pp. 1–66). Neill.
- Heath, T. A., Huelsenbeck, J. P., & Stadler, T.** (2014). The fossilized birth-death process for coherent calibration of divergence-time estimates. *Proceedings of the National Academy of Science*, 111, 2957–2966. <https://doi.org/10.1073/pnas.1319091111>
- Hecht, T.** (1982). On the enigmatic sagittal otoliths and the systematic position of the teleostean genera *Adioryx*, *Holocentrus* and *Flammeo* (Beryciformes: Holocentridae). *Israel Journal of Zoology*, 31, 39–46. <https://doi.org/10.1080/00212210.1982.10688519>
- Higgins, M. W., & Conant, L. B.** (1986). *Geologic map of Cecil County. Scale 1:62,500*. Maryland Geological Survey.
- Houttuyn, M.** (1782). Beschryving van eenige Japansche visschen, en andere zee-schepzelen. *Natuurkundige verhandelingen van de Bataafsche Hollandsche Maatschappye der Wetenschappen te Haarlem*, 20, 331–350.
- Huelsenbeck, J. P., & Ronquist, F.** (2001). MRBAYES: Bayesian inference of phylogenetic trees. *Bioinformatics*, 17, 754–755. <https://doi.org/10.1093/bioinformatics/17.8.754>
- Hughes, L. C., Ortí, G., Huang, Y., Sun, Y., Baldwin, C. C., Thompson, A. W., Arcila, D., Betancur-R., R., Li, C., Becker, L., Bellora, N., Zhao, X., Li, X., Wang, M., Fang, C., Xie, B., Zhou, Z., Huang, H., Chen, S., Venkatesh, B., & Shi, Q.** (2018). Comprehensive phylogeny of ray-finned fishes (Actinopterygii) based on transcriptomic and genomic data. *Proceedings of the National Academy of Science*, 115, 6249–6254. <https://doi.org/10.1073/pnas.1719358115>
- Hughes, L. C., Ortí, G., Huang, Y., Sun, Y., Baldwin, C. C., Thompson, A. W., Arcila, D., Betancur-R., R., Li, C., Becker, L., Bellora, N., Zhao, X., Li, X., Wang, M., Fang, C., Xie, B., Zhou, Z., Huang, H., Chen, S., Venkatesh, B., & Shi, Q.** (2019). *Comprehensive phylogeny of ray-finned fishes (Actinopterygii) based on transcriptomic and genomic data* [Data set]. Dryad. <https://doi.org/10.5061/dryad.5b85783>
- Johnson, D. G., & Patterson, C.** (1993). Percomorph phylogeny: a survey of acanthomorphs and a new proposal. *Bulletin of Marine Science*, 52, 554–626.
- Kennedy, W. J., & Cobban, W. A.** (1996). Maastrichtian ammonites from the Hornerstown Formation in New Jersey. *Journal of Paleontology*, 70, 798–804.
- Koch, R. C., & Olsson, R. K.** (1977). Dinoflagellate and planktonic foraminiferal biostratigraphy of the uppermost Cretaceous of New Jersey. *Journal of Paleontology*, 51, 480–491.
- Lanfear, R., Calcott, B., Ho, S. Y., & Guindon, S.** (2012). PartitionFinder: combined selection of partitioning schemes and substitution models for phylogenetic analyses. *Molecular Biology and Evolution*, 29, 1695–1701. <https://doi.org/10.1093/molbev/mss020>
- Lanfear, R., Frandsen, P. B., Wright, A. M., Senfeld, T., & Calcott, B.** (2017). PartitionFinder 2: New methods for selecting partitioned models of evolution for molecular and morphological phylogenetic analyses. *Molecular Biology and Evolution*, 34, 772–773. <https://doi.org/10.1093/molbev/msw260>
- Larsson, A.** (2014). AliView: a fast and lightweight alignment viewer and editor for large data sets. *Bioinformatics*, 30, 3276–3278. <https://doi.org/10.1093/bioinformatics/btu531>
- Lewis, P. O.** (2001). A likelihood approach to estimating phylogeny from discrete morphological character data. *Systematic Biology*, 50, 913–925. <https://doi.org/10.1080/106351501753462876>
- López-Palomino, I., González-Rodríguez, K. A., Schultze, H. P., Palma-Ramírez, A., & Contreras-Cruz, D.** (2021). Ammonites from the La Negra Facies (El Doctor Formation, late Albian) of the Muhi Quarry, Hidalgo, central Mexico. *Journal of South American Earth Sciences*, 111, 103400. <https://doi.org/10.1016/j.jsames.2021.103400>
- Lowe, R. T.** (1834). Characters of a new genus Leirus, and of several new species from Madeira. *Proceedings of the Zoological Society of London*, 1833, 142–144.
- Maddison, D. R., & Maddison, W. P.** (2000). *MacClade: Analysis of phylogeny and character evolution*. Sinauer, Sunderland.
- Mantell, G. A.** (1822). *The fossils of the South Downs or illustrations of the geology of Sussex*. Lupton Relfe.
- Marramà, G., Giusberti, L., Papazzoni, C. A., & Carnevale, G.** (2021). An Eocene soldierfish (Teleostei: Holocentridae) from Monte Baldo (NE Italy). *Bollettino della Società Paleontologica Italiana*, 60, 135–147. <https://doi.org/10.4435/BSPI.2021.12>
- Miller, M. A., Pfeiffer, W., & Schwartz, T.** (2010). Creating the CIPRES Science Gateway for inference of large phylogenetic trees. *Proceedings of the Gateway*

- Computing Environments Workshop*, New Orleans, 1–8. <https://doi.org/10.1109/GCE.2010.5676129>
- Miya, M., Takeshima, H., Endo, H., Ishiguro, N. B., Inoue, J. G., Mukai, T., Satoh, T. P., Yamaguchi, M., Kawaguchi, A., Mabuchi, K., Shirai, S. M., & Nishida, M. (2003). Major patterns of higher teleostean phylogenies: a new perspective based on 100 complete mitochondrial DNA sequences. *Molecular Phylogenetics and Evolution*, 26, 121–138. [https://doi.org/10.1016/s1055-7903\(02\)00332-9](https://doi.org/10.1016/s1055-7903(02)00332-9)
- Moore, J. A. (1993). Phylogeny of the Trachichthyiformes (Teleostei: Percomorpha). *Bulletin of Marine Science*, 52, 114–136.
- Müller, J. P. (1845). Über den Bau und die Grenzen der Ganoiden, und über das natürliche System der Fische. *Archiv für Naturgeschichte*, 11, 91–141.
- Murray, A. M. (2016). Mid-Cretaceous acanthomorph fishes with a description of a new species from the Turonian of Lac de Bois, Northwest Territories, Canada. *Vertebrate Anatomy and Morphology*, 1, 101–115. <https://doi.org/10.18435/B5CC78>
- Murray, A. M., Brinkman, D. B., Newbrey, M. G., & Neuman, A. G. (2020). Earliest North American articulated freshwater acanthomorph fish (Teleostei: Percopsiformes) from Upper Cretaceous deposits of Alberta, Canada. *Geological Magazine*, 157, 1087–1096. <https://doi.org/10.1017/S0016756819001328>
- Nelson, E. M. (1955). The morphology of the swim bladder and auditory bulla in the Holocentridae. *Fieldiana, Zoology*, 37, 121–130.
- Nelson, J. S., Grande, T. C., & Wilson, M. V. H. (2016). *Fishes of the World*, 5th Edition. John Wiley & Sons. <https://doi.org/10.1002/9781119174844>
- Nolf, D. (2013). *The diversity of fish otoliths, past and present*. Royal Belgian Institute of Natural Sciences.
- Obasi, C. C., Terry, D. O. Jr, Myer, G. H., & Grandstaff, D. E. (2011). Glauconite composition and morphology, shocked quartz, and the origin of the Cretaceous(?) Main Fossiliferous Layer (MFL) in Southern New Jersey, USA. *Journal of Sedimentary Research*, 81, 479–494. <https://doi.org/10.2110/jsr.2011.42>
- Owens, J. P., & Sohl, N. F. (1973). Glauconites from New Jersey-Maryland coastal plain: their K-Ar ages and application in stratigraphic studies. *Geological Society of America Bulletin*, 84, 2811–2838.
- Owens, J. P., Sugarman, P. J., Sohl, N. F., Parker, R. A., Houghton, H. F., Volkert, R. A., Drake, A. A., & Orndorff, R. C. (1999). *Bedrock geological map of central and southern New Jersey. Scale 1 to 100,000*. US Geological Survey.
- Parris, D. C. (1974). Additional records of plesiosaurs from the Cretaceous of New Jersey. *Journal of Paleontology*, 48, 32–35.
- Patterson, C. (1964). A review of Mesozoic acanthopterygian fishes, with special reference to those of the English Chalk. *Philosophical Transactions of the Royal Society, London*, 247, 213–482. <https://doi.org/10.1098/rstb.1964.0003>
- Patterson, C. (1967). New Cretaceous berycoid fishes from the Lebanon. *Bulletin of the British Museum of Natural History (Geology)*, 14, 67–110.
- Patterson, C. (1968). The caudal skeleton in Mesozoic acanthopterygian fishes. *Bulletin of the British Museum of Natural History (Geology)*, 17, 47–102.
- Patterson, C. (1993). An overview of the early fossil record of acanthomorphs. *Bulletin of Marine Science*, 52, 29–59.
- Patterson, C., & Rosen, D. E. (1977). Review of Ichthyodectiform and other Mesozoic teleost fishes and the theory and practice of classifying fossils. *Bulletin of the American Museum of Natural History*, 158, 81–172.
- Price, S. A., Schmitz, L., Oufiero, C. E., Eytan, R. I., Dornburg, A., Smith, W. L., Friedman, M., Near, T. J., & Wainwright, P. C. (2014). Two waves of colonization straddling the K-Pg boundary formed the modern reef fish fauna. *Proceedings of the Royal Society B*, 281, 20140321. <https://doi.org/10.1098/rspb.2014.0321>
- Rabosky, D. L., Chang, J., Title, P. O., Cowman, P. F., Sallan, L., Friedman, M., Kaschner, K., Garilao, C., Near, T. J., Coll, M., & Alfaro, M. E. (2018). An inverse latitudinal gradient in speciation rate for marine fishes. *Nature*, 559, 392–395. <https://doi.org/10.1038/s41586-018-0273-1>
- Rambaut, A., Drummond, A. J., Xie, D., Baele, G., & Suchard, M. A. (2018). Posterior summarisation in Bayesian phylogenetics using Tracer 1.7. *Systematic Biology*, 67, 901–904. <https://doi.org/10.1093/sysbio/syy032>
- Randall, J. E., Shimizu, T., & Yamakawa, T. (1982). A revision of the holocentrid fish genus *Ostichthys*, with descriptions of four new species and a related new genus. *Japanese Journal of Ichthyology*, 29, 1–26.
- Rapp, W. F. (1946). Check list of the fossil fishes of New Jersey. *Journal of Paleontology*, 20, 510–513.
- Regan, C. T. (1911). I. – The anatomy and classification of the Teleostean fishes of the orders Berycomorphi and Xenoberyces. *Annals and Magazine of Natural History*, 7, 1–9.
- Reichenbacher, B., Seinknecht, U., Küchenhoff, H., & Fenske, N. (2007). Combined otolith morphology and morphometry for assessing taxonomy and diversity in fossil and extant killifish (*Aphanius*, †*Prolebias*). *Journal of Morphology*, 268, 898–915. <https://doi.org/10.1002/jmor.10561>
- Renema, W., Bellwood, D. R., Braga, J. C., Bromfield, K., Hall, R., Johnson, K. G., Lunt, P., Meyer, C. P., McMonagle, L. B., Morley, R. J., O’Dea, A., Todd, J. A., Wesselingh, F. P., Wilson, M. E. J., & Pandolfi, J. M. (2008). Hopping hotspots: Global shifts in marine biodiversity. *Science*, 321, 654–657. <https://doi.org/10.1126/science.1155674>
- Richardson, J. (1846). Report on the ichthyology of the seas of China and Japan. *Report of the British Association for the Advancement of Science*, 1845, 187–320.
- Rosen, D. E. (1973). Interrelationships of higher euteleostean fishes. In P. H. Greenwood, Miles S., & Patterson C. (Eds.), *Interrelationships of Fishes* (pp. 397–513). Academic Press.
- Sabaj, M. H. (2020). Codes for natural history collections in ichthyology and herpetology. *Ichthyology & Herpetology*, 108, 593–669. <https://doi.org/10.1643/ASIHCODONS2020>
- Saulsbury, J. G., & Baumiller, T. K. (2022). Dispersals from the West Tethys as the source of the Indo-West Pacific diversity hotspot in comatulid crinoids. *Paleobiology, First View*, 1–14. <https://doi.org/10.1017/pab.2022.23>
- Schwarzahns, W. (1978). Otolith-morphology and its usage for higher systematical units, with special reference to the Myctophiformes s.l. *Mededelingen van de Werkgroep voor Tertiaire en Kwartaire Geologie*, 15, 167–185.

- Schwarzahns, W.** (2010). Otolithen aus den Gerhartsreiter Schichten (Oberkreide: Maastricht) des Gerhartsreiter Grabens (Oberbayern). *Palaeo Ichthyologica*, 4, 1–100.
- Schwarzahns, W., Beckett, H. T., Schein, J. D., & Friedman, M.** (2018). Computed tomography scanning as a tool for linking the skeletal and otolith-based fossil records of teleost fishes. *Palaeontology*, 61, 511–541. <https://doi.org/10.1111/pala.12349>
- Schwarzahns, W., Schulz-Mirbach, T., Lombarte, A., & Tuset, V. M.** (2017). The origination and rise of teleost otolith diversity during the Mesozoic. *Research & Knowledge*, 3, 5–8. <https://doi.org/10.14456/randk.2017.2>
- Sibert, E. C., & Norris, R. D.** (2015). New Age of Fishes initiated by the Cretaceous–Paleogene mass extinction. *Proceedings of the National Academy of Sciences*, 112, 8537–8542. <https://doi.org/10.1073/pnas.1504985112>
- Siqueira, A. C., Bellwood, D. R., & Cowman, P. F.** (2019). Historical biogeography of herbivorous coral reef fishes: the formation of an Atlantic fauna. *Journal of Biogeography*, 46, 1611–1624. <https://doi.org/10.1111/jbi.13631>
- Sorbini, L.** (1975a). Gli Holocentridae di Monte Bolca. I: Eoholocentrum, nov. gen., Eoholocentrum macrocephalum (de Blainville) (Pisces). *Studi e Ricerche sui Giacimenti Terziari di Bolca*, 2, 205–228.
- Sorbini, L.** (1975b). Gli Holocentridae di Monte Bolca. II: *Tenuicentrum patternsoni* nov. gen. nov. sp. Nuovi dati a favore dell'origine monofiletica dei Beryciformei (Pisces). *Studi e Ricerche sui Giacimenti Terziari di Bolca*, 2, 455–472.
- Sorbini, L.** (1979a). Les Holocentridae du Monte Bolca. III: *Berybolcensis leptacanthus* (Agassiz). *Studi e Ricerche sui Giacimenti Terziari di Bolca*, 4, 19–35.
- Sorbini, L.** (1979b). Resultats de la revision de Beryciformes et des Perciformes generalizes du Monte Bolca. *Studi e Ricerche sui Giacimenti Terziari di Bolca*, 4, 41–48.
- Sorbini, L., & Tirapelle, R.** (1975). Gli Holocentridae di Monte Bolca. I: Eoholocentrum, nov. gen., Eoholocentrum macrocephalum (de Blainville) (Pisces-Actinopterygii). *Studi e Ricerche sui Giacimenti Terziari di Bolca*, 2, 143–154.
- Spix, J. B., Agassiz, L., & Martius, K. L. P.** (1829–1831). *Selecta genera et species piscium: quos in itinere per Brasiliam annis MDCCCXVII–MDCCCXX jussu et auspiciis Maximiliani Josephi I. Typis C. Wolf.*
- Staron, R. M., Grandstaff, B. S., Gallagher, W. B., & Grandstaff, D. E.** (2001). REE signatures in vertebrate fossils from Sewell, NJ: Implications for location of the K-T boundary. *PALAIOS*, 16, 255–265. <https://doi.org/10.2307/3515603>
- Steindachner, F., & Döderlein, L.** (1883). Beiträge zur Kenntniss Der Fische Japans. *Denkschriften Akademie der Wissenschaften in Wien*, 47, 211–242.
- Stewart, J. D.** (1984). *Taxonomy, paleoecology, and stratigraphy of the halecostome-inoceramid associations of the North American Upper Cretaceous epicontinental seaways* [Unpublished PhD thesis]. University of Kansas.
- Stewart, J. D.** (1996). Cretaceous acanthomorphs of North America. In G. Arratia & G. Viohl (Eds.), *Mesozoic fishes: Systematics and paleoecology* (pp. 383–394). Friedrich Pfeil.
- Stiassny, M. L., & Moore, J. A.** (1992). A review of the pelvic girdle of acanthomorph fishes, with comments on hypotheses of acanthomorph intrarelationships. *Zoological Journal of the Linnean Society*, 104, 209–242.
- Swofford, D. L.** (2003). *PAUP\*. Phylogenetic analysis using parsimony (\* and other methods) v4*. Sinauer Associates.
- Tomlinson, J. L., & Ramsey, K. W.** (2020). *Geologic map of the Cecilton and Middletown Quadrangles, Delaware. Scale 1:24,000*. Delaware Geological Survey.
- Tuset, V. M., Farré, M., Otero-Ferrer, J. L., Vilar, A., Morales-Nin, B., & Lombarte, A.** (2016). Testing otolith morphology for measuring marine fish biodiversity. *Marine and Freshwater Research*, 67, 1037–1048. <https://doi.org/10.1071/MF15052>
- Ullmann, P. V., Boles, Z. M., & Knell, M. J.** (2018). Insights into cranial morphology and intraspecific variation from a new subadult specimen of the pancheloniid turtle *Euclastes wielandi* Hay, 1908. *PaleoBios*, 35, 1–22. <https://doi.org/10.5070/P9351042081>
- Ullmann, P. V., & Carr, E.** (2021). *Catapleura* Cope, 1870 is *Euclastes* Copes, 1867 (Testudines: Pan-Chelonidae): synonymy revealed by a new specimen from New Jersey. *Journal of Systematic Palaeontology*, 19, 491–517. <https://doi.org/10.1080/14772019.2021.1928306>
- Voegele, K. K., Ullmann, P. V., Lonsdorf, T., Christmas, Z., Heierbacher, M., Kibelstis, B. J., Putnam, I., Boles, Z. M., Walsh, S., & Lacovara, K. J.** (2021). Microstratigraphic analysis of fossil distribution in the lower Hornerstown and upper Navesink formations at the Edelman Fossil Park, NJ. *Frontiers in Earth Science*, 9, 756655. <https://doi.org/10.3389/feart.2021.756655>
- Walbaum, J. J.** (1792). *Petri Artdi sueci genera piscium. In quibus systema totum ichthyologiae proponitur cum classibus, ordinibus, generum characteribus, specierum differentiis, observationibus plurimis. Redactis speciebus 242 ad genera 52. Ichthyologiae pars III.* Ant. Ferdin. Rose.
- Whitley, G. P.** (1941). Ichthyological notes and illustrations. *The Australian Zoologist*, 10, 1–50.
- Wisniewski, A. L., Lloyd, G. T., & Slater, G. J.** (2022). Extant species fail to estimate ancestral geographical ranges at older nodes in primate phylogeny. *Proceedings of the Royal Society B*, 289, 20212535. <https://doi.org/10.1098/rspb.2021.2535>
- Woods, L. P., & Sonoda, P. M.** (1973). Order Berycimorphi (Beryciformes). In D. M. Cohen, A. W. Ebeling, T. Iwamoto, S. B. McDowell, N. B. Marshall, D. E. Rosen, P. Sonoda, W. H. Weed, L. P. Woods (Eds.), *Fishes of the Western North Atlantic 1* (pp. 263–396). Sears Foundation for Marine Research <https://doi.org/10.2307/j.ctvbc0bn>.
- Woodward, A. S.** (1887). VI. – On a new species of Holocentrum from the Miocene of Malta; with a list of fossil Berycidae hitherto described. *Geological Magazine*, 4, 355–359. <https://doi.org/10.1017/S0016756800193963>
- Woodward, A. S.** (1903). The fossils of the English Chalk. *Palaeontological Society of London*, 2, 57–96.
- Zehren, S. J.** (1979). *The comparative osteology and phylogeny of the Beryciformes (Pisces: Teleostei)*. Evolutionary Monographs.
- Zhang, C., Stadler, T., Klopffstein, S., Heath, T. A., & Ronquist, F.** (2016). Total-evidence dating under the Fossilized Birth-Death Process. *Systematic Biology*, 65, 228–249. <https://doi.org/10.1093/sysbio/syv080>